Inorg. Chem. **2005**, *44*, 3636–3656

Square Planar vs Tetrahedral Coordination in Diamagnetic Complexes of Nickel(II) Containing Two Bidentate π-Radical Monoanions

Sebastien Blanchard, Frank Neese, Eberhard Bothe, Eckhard Bill, Thomas Weyhermüller, and Karl Wieghardt*

Max-Planck-Institut für Bioanorganische Chemie, Stiftstrasse 34-36, D-45470 Mülheim an der Ruhr, Germany

Received October 18, 2004

The reaction of three different 1-phenyl and 1,4-diphenyl substituted *S*-methylisothiosemicarbazides, $H_2[L^{1-6}]$, with $Ni(OAc)_2 \cdot 4H_2O$ in ethanol in the presence of air yields six four-coordinate species $[Ni(L^{1-6\bullet})_2]$ (**1**–**6**) where $(L^{1-6\bullet})^{1-}$ represent the monoanionic π-radical forms. The crystal structures of the nickel complexes with 1-phenyl derivatives as in **1** reveal a square planar structure *trans*-$[Ni(L^{1-3\bullet})_2]$, whereas the corresponding 1,4-diphenyl derivatives are distorted tetrahedral as is demonstrated by X-ray crystallography of $[Ni(L^{5\bullet})_2]$ (**5**) and $[Ni(L^{6\bullet})_2]$ (**6**). Both series of mononuclear complexes possess a diamagnetic ground state. The electronic structures of both series have been elucidated experimentally (electronic spectra magnetization data). The square planar complexes **1**–**3** consist of a diamagnetic central Ni(II) ion and two strongly antiferromagnetically coupled ligand π-radicals as has been deduced from correlated ab initio calculations; they are singlet diradicals. The tetrahedral complexes **4**–**6** consist of a paramagnetic high-spin Ni^{II} ion ($S_{Ni} = 1$), which is strongly antiferromagnetically coupled to two ligand π-radicals. This is clearly revealed by DFT and correlated ab initio calculations. Electrochemically, complexes **1**–**6** can be reduced to form stable, paramagnetic monoanions $[\mathbf{1}–\mathbf{6}]^-$ ($S = {}^1/_2$). The anions $[\mathbf{1}–\mathbf{3}]^-$ are square planar Ni(II) (d^8, $S_{Ni} = 0$) species where the excess electron is delocalized over both ligands (class III, ligand mixed valency). In contrast, one-electron reduction of **4**, **5**, and **6** yields paramagnetic *tetrahedral* monoanions ($S = {}^1/_2$). X-band EPR spectroscopy shows that there are two different isomers A and B of each monoanion present in solution. In these anions, the excess electron is localized on one ligand $[Ni^{II}(L^{4-6\bullet})(L^{4-6})]^-$ where $(L^{4-6})^{2-}$ is the closed shell dianion of the ligands $H_2[L^{4-6}]$ as was deduced from their electronic spectra and broken symmetry DFT calculations. Oxidation of **1** and **5** with excess iodine yields octahedral complexes $[Ni^{II}(L^{1,ox})_2I_2]$ (**7**), $[Ni^{II}(L^{1,ox})_3](I_3)_2$ (**8**), and *trans*-$[Ni^{II}(L^{5,ox})_2(I_3)_2]$ (**9**), which have been characterized by X-ray crystallography; $(L^{1-6,ox})$ represent the neutral, two-electron oxidized forms of the corresponding dianions $(L^{1-6})^{2-}$. The room-temperature structures of complexes **1**, **5**, and **7** have been described previously in refs 1–5.

Introduction

Revenco and Gerbeleu et al.[1–5] have reported in a series of elegant papers on the coordination chemistry of *S*-methyl-1-phenyl-isothiosemicarbazides and of the sterically more demanding *S*-methyl-1,4-diphenyl-isothiosemicarbazides with nickel(II) and cobalt(III) ions. Scheme 1 displays the structures of these ligands and gives their abbreviations.

The doubly deprotonated forms of the neutral molecules, $(L^x)^{2-}$, could, in principle, act as bidentate dianionic ligands in transition metal ion complexes generating five-membered chelate rings.

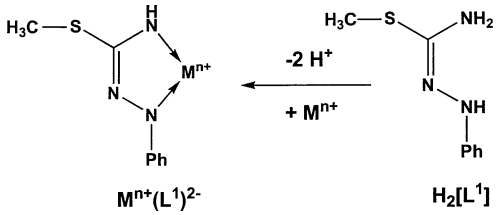

$M^{n+}(L^1)^{2-}$ $H_2[L^1]$

However, such species have not been observed to date, but their oxidized monoanions which are paramagnetic

* To whom correspondence should be addressed. E-mail: wieghardt@mpi-muelheim.mpg.de.

(1) (a) Simonov, Y. A.; Revenco, M. D.; Bourosh, P. N.; Gerbeleu, N. V.; Vyrtosu, N. I.; Indrichan, K. M.; Chumakov, Y. M.; Bel'skii, V. K. *Dokl. Akad. Nauk SSSR* **1988**, *298*, 378−82. (b) Revenco, M. D.; Simonov, Y. A.; Vyrtosu, N. I.; Gerbeleu, N. V.; Bourosh, P. N.; Bel'skii, V. K.; Indrichan, K. M. *Zh. Neorg. Khim.* **1988**, *33*, 2049.

10.1021/ic040117e CCC: $30.25 © 2005 American Chemical Society
Published on Web 04/16/2005

Scheme 1. Ligands and Abbreviations

Ligands

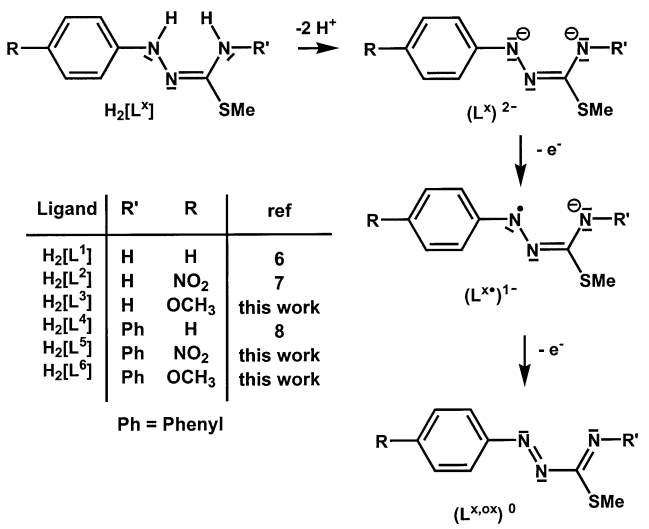

Ligand	R'	R	ref
$H_2[L^1]$	H	H	6
$H_2[L^2]$	H	NO_2	7
$H_2[L^3]$	H	OCH_3	this work
$H_2[L^4]$	Ph	H	8
$H_2[L^5]$	Ph	NO_2	this work
$H_2[L^6]$	Ph	OCH_3	this work

Ph = Phenyl

π-radicals ($S_{rad} = {}^1/_2$), namely, $(L^x)^{1-\bullet}$, have been identified in diamagnetic, square planar $[Ni^{II}(L^{1\bullet})_2]$ (**1**).[1] These π-radical anions have also been identified by X-ray crystallography in $[Co^{III}(L^{1\bullet})_2I]$[5] and in $[Fe^{III}(L^{1\bullet})_2X]$ (X = Cl, CH_3S).[6]

Interestingly, square planar **1** can be oxidized by iodine yielding paramagnetic, octahedral *trans*-$[Ni^{II}(L^{1,ox})_2I_2]$ (**7**) (S = 1) the crystal structure of which has been determined[2] at ambient temperature (Scheme 2). We have discovered here that oxidation of **1** can also afford paramagnetic $[Ni^{II}(L^{1,ox})_3]$-$(I_3)_2$ (**8**), which we have characterized structurally.

In all of these complexes, the two C−N and the N−N bond lengths of each five-membered chelate ring are characteristic for the oxidation level of the ligand as either $(L^{x\bullet})^{1-}$ or $(L^{x,ox})^0$. For example, in complexes with $(L^{x\bullet})^{1-}$ π-radicals the N−N bond is rather short at 1.34 ± 0.01 Å but significantly shorter at 1.24 ± 0.01 Å in complexes containing the $(L^{x,ox})$ form. Thus, high-quality X-ray crystallography is an efficient tool to assign the given ligand oxidation level. Since the structures of **1** and **7** (Scheme 3) have been determined at room temperature only, we decided to redetermine their structures by using new data sets collected at 100(2) K. The estimated standard deviations are significantly smaller.

Most importantly, Revenco and Gerbeleu et al.[3,4] reported in two papers the synthesis and crystal structures of two such nickel(II) complexes containing each two π-radical monoanions of the ligands $H_2(L^5)$ and phenylazothiomethyl-(2-methoxy-phenylimino)methane shown in Figure 1. Both complexes, $[Ni^{II}(L^{5\bullet})_2]$ (**5**) and $[Ni^{II}(L_{Ph}^{OCH_3\bullet})_2]$ are diamagnetic, but they possess a distorted *tetrahedral* N_4-donor set. Thus, the spin coupling yielding the S = 0 ground state must be different from that in the corresponding square planar complexes. The authors imply that this structural difference is a consequence of the presence of a second N-phenyl group in these two ligands, which is suggested to lead to an

Scheme 2. Syntheses of **1** and **2** According to Ref 2

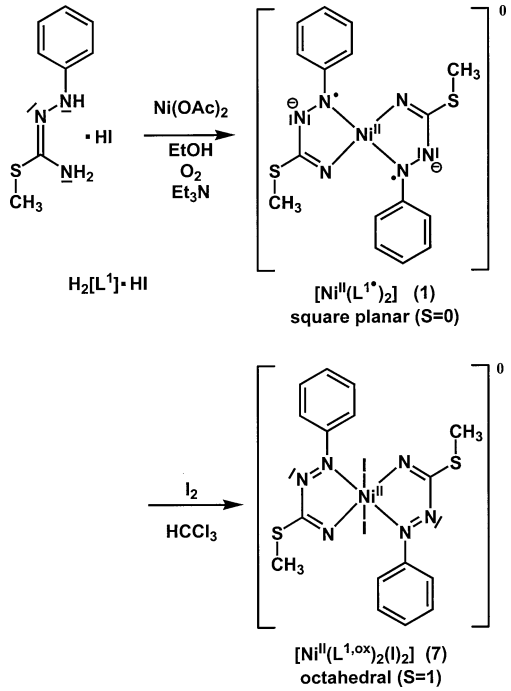

Scheme 3. Complexes of This Work[a]

Complex	No.	geometry	S[a)]	Ref.
$[Ni(L^{1\bullet})_2]$	1	s. pl.[b)]	S=0	ref. 1
$[Ni(L^{2\bullet})_2]$	2	s. pl.	S=0	this work
$[Ni(L^{3\bullet})_2]$	3	s. pl.	S=0	this work
$[Ni(L^{4\bullet})_2]$	4	tetr.[c)]	S=0	ref. 1b
$[Ni(L^{5\bullet})_2]$	5	tetr.	S=0	ref. 3
$[Ni(L^{6\bullet})_2]$	6	tetr.	S=0	this work
$[Ni(L^{1,ox})_2I_2]$	7	oct.[d)]	S=1	ref. 2
$[Ni(L^{1,ox})_3](I_3)_2$	8	oct.	S=1	this work
$[Ni(L^{5,ox})_2(I_3)_2]$	9	oct.	S=1	this work

[a] (a) Ground state; (b) s. pl. = square planar geometry at Ni^{II}; (c) tetr. = tetrahedral geometry at Ni^{II}; (d) oct. = octahedral geometry at Ni^{II}.

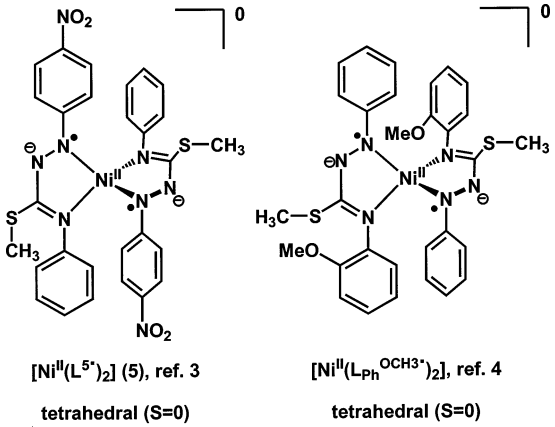

Figure 1. Diamagnetic tetrahedral complexes of **5** from ref 3 and $[Ni^{II}(L_{Ph}^{OCH_3\bullet})_2]$ from ref 4.

(2) Revenco, M. D.; Vyrtosu, N. I.; Gerbeleu, N. V.; Simonov, Y. A.; Bourosh, P. N.; Sobolev, A. N. *Zh. Neorg. Khim.* **1988**, *33*, 2353.
(3) Simonov, Y. A.; Battaglia, L. P.; Corradi, A. B.; Pelosi, G.; Revenco, M. D.; Gerbeleu, N. V. *Acta Crystallogr.* **1991**, *C47*, 1826.
(4) Bourosh, P. N.; Revenco, M. D.; Timco, L. A.; Simonov, Y. A. *Zh. Neorg. Khim.* **1999**, *44*, 1258.
(5) Revenco, M. D.; Gerbeleu, N. V.; Simonov, Y. A.; Bourosh, P. N.; Vyrtosu, N. I.; Sobolev, A. N.; Malinovskii, T. I. *Dokl. Akad. Nauk SSSR* **1988**, *300*, 127.
(6) Blanchard, S.; Bill, E.; Weyhermüller, T.; Wieghardt, K. *Inorg. Chem.* **2003**, *43*, 2324.

Scheme 4. Ligand Oxidation Products

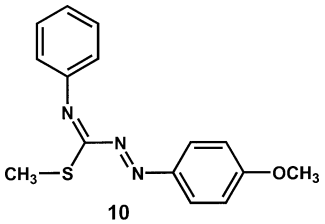

10

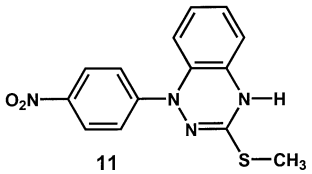

11

increased steric bulk as compared to those complexes with two ligands having each only a single N-phenyl group ($H_2[L^{1-3}]$).

To the best of our knowledge, there are only two other tetrahedral complexes with an S = 0 ground state containing a central nickel(II) ion and two π-radical monoanions known. Pierpont et al.[7] reported the structure of tetrahedral, diamagnetic $[Ni^{II}(PhenoxSQ)_2]$ (PhenoxBQ = 2,4,6,8-tetra-*tert*-butylphenoxazin-1-one and $(PhenoxSQ)^{1-\bullet}$ is its one-electron reduced semiquinone form), and Hazell[8] reported the tetrahedral structure of diamagnetic bis(*N*,*N*-diethyl-phenylazothioformamide)nickel(II), $[Ni\{(C_6H_5)NNCSN(C_2H_5)_2\}_2]$, where the corresponding Zn(II) complex possesses an S = 1 ground state[9] verifying the π-radical anion character of the coordinated ligands.

Our present results indicate clearly that the oxidation of diamagnetic, tetrahedral $[Ni(L^{5\bullet})_2]$ (**5**) with excess iodine yields paramagnetic, octahedral *trans*-$[Ni^{II}(L^{5,ox})_2(I_3)_2]$ (**9**), where the two ligands $(L^{5,ox})^0$ are coordinated in *trans*-position relative to each other with a planar NiN_4 moiety. Thus, in this case no or only weak steric repulsion between the ligands appears to exist.

We have synthesized here a series of new *S*-methyl-1-phenyl-isothiosemicarbazones $H_2[L^2]$, $H_2[L^3]$ and also their 1,4-diphenyl derivatives $H_2[L^{4-6}]$ (Scheme 1) and prepared the diamagnetic nickel(II) complexes **1**−**6** shown in Scheme 3. From spectroscopic characterizations and X-ray structure determinations, it is shown that complexes **1**, **2**, and **3** are square planar molecules, whereas in **4**, **5**, and **6** the nickel(II) ion is in a tetrahedral environment. Here we also present density functional theoretical (DFT) and correlated ab initio calculations on these neutral square planar and tetrahedral complexes and their monoreduced forms.

Finally, we have isolated and characterized two different ligand oxidation products of the ligands $H_2[L^5]$ and $H_2[L^6]$ shown in Scheme 4.

Experimental Section

p-Methoxyphenylhydrazine hydrochloride, phenylhydrazine hydrochloride, ammonium thiocyanate, methyl iodide, *p*-nitroaniline, sodium nitrite, phenyl isothiocyanate, and $Ni(OAc)_2 \cdot 4H_2O$ were purchased from Aldrich. All chemicals were used without further purification. The synthesis of *S*-methyl-1-phenyl-isothiosemicarbazide hydroiodide $H_2[L^1] \cdot HI$ has been described elsewhere.[6] *p*-Nitrophenylhydrazine hydrochloride was prepared according to published literature.[10]

***S*-Methyl-1-*p*-nitrophenyl-isothiosemicarbazide Hydroiodide, $H_2[L^2] \cdot HI$.** Starting from *p*-nitrophenylhydrazine hydrochloride and ammonium thiocyanate, 1-*p*-nitrophenyl-isothiosemicarbazide was obtained in 82% yield according to a published procedure.[11] EI-MS: $m/z = 212$ for $\{C_7H_8N_4O_2S\}^+$. ^{1}H NMR (400 MHz, DMSO-d_6): δ(ppm) = 6.71 (d, J = 9.6 Hz, 2H, *o*-HArNN), 7.67 (br s, 1H, C(S)NH_2), 7.94 (br s, 1H, C(S)NH_2), 8.10 (d, J = 9.6 Hz, 2H, *m*-HArNN), 9.06 (s, 1H, ArNH), 9.54, (s, 1H, ArNNH); ^{13}C NMR (400 MHz, DMSO-d_6): δ(ppm) = 111.2 (CH, *o*-ArNN), 125.8 (CH, *p*-ArNN), 138.8 (Cq, *p*-ArNN), 154.0 (Cq, ArNN), 182.5 (Cq, C=S).

1-*p*-Nitrophenyl-isothiosemicarbazide (5.24 g, 24.6 mmol) was suspended in absolute ethanol (150 mL) and methyl iodide (1.53 mL, 3.49 g, 24.6 mmol) was added. After heating of the dark red solution for 2 h, the solvent was removed by evaporation and the orange powder was suspended in dichloromethane (20 mL). The precipitate was filtered off and washed with dichloromethane (2.5 mL). Yield: 7.36 g (85%). EI-MS: $m/z = 226$ for $\{C_8H_{11}N_4O_2S\}^+$. As was observed in the case of *S*-methyl-1-phenyl-isothiosemicarbazide hydroiodide,[6] the ^{1}H NMR (400 MHz, DMSO-d_6, 300 K) spectrum corresponds to that of two tautomers in equilibrium, in a 85/15 ratio (M = major isomer, m = minor isomer): δ(ppm) = 2.48 (s, 0.45 H, SMe(m)), 2.72 (s, 2.55 H, SMe(M), 6.92 (d, 2H, J = 5.2 Hz, *o*-HArNN), 8.17 (d, 2H, J = 5.2 Hz, *m*-HArNN), 9.48 (s, 0.85 H, ArNHN(M)), 9.57 (br s, NH), 9.60 (s, 0.15 H, ArNHN(m)), 11.39 (br s, NH). ^{13}C NMR (400 MHz, DMSO-d_6, 300 K): δ(ppm) = 12.7 (CH_3, SMe(m)), 13.3 (CH_3, SMe(M)), 112 (CH, *o*-ArNN), 125.7 (CH, *p*-ArNN), 140.0 (Cq, *p*-ArNN(M)), 140.3 (Cq, *p*-ArNN(m)), 152.0 (Cq, ArNN(M)), 152.2 (Cq, ArNN(m)), 170 (Cq, C=S).

***S*-Methyl-1-*p*-methoxyphenyl-isothiosemicarbazide Hydroiodide, $H_2[L^3] \cdot HI$.** Using the same procedure as for 1-*p*-nitrophenylisothiosemicarbazide, we obtained a ca. 80:20 mixture of the tautomers in the 1- and 2-positions of *p*-methoxyphenyl-isothiosemicarbazide. These two products could not easily be separated; therefore, we performed the methylation step on the mixture. *p*-Methoxyphenyl-isothiosemicarbazide (5.6 g, 27.7 mmol) was suspended in absolute ethanol (150 mL), and then methyliodide was added (1.73 mL, 3.95 g, 27.7 mmol) and the mixture was heated to reflux for 2 h. After cooling of the sample to room temperature, a white powder was filtered off. Recrystallization from dichloromethane at −30 °C yielded 3.55 g (37%) of pure pale yellow $H_2[L^3] \cdot HI$. ESI-MS (MeOH; pos. ion): $m/z = 212$ for $\{C_9H_{14}N_3OS\}^+$. Coalescence processes in variable temperature ^{1}H NMR (400 MHz, DMSO-d_6, 300−340 K) experiments prove that two tautomers are in equilibrium in solution, with a 80:20 ratio at 300 K; ^{1}H NMR (400 MHz, DMSO-d_6, 300 K, M = major isomer only, m = minor isomer only): δ(ppm) = 2.49 (s, 0.6 H, SMe(m)), 2.68 (s, 2.4 H, SMe(M)), 3.65 (s, 0.6 H, OMe(m)), 3.68 (s, 2.4 H, OMe(M)), 6.76 (m, 2H, *o*-HArNN), 6.86 (m, 2H, *m*-HArNN), 8.15 (s, 0.8 H, ArNHN(M)), 8.27 (s, 0.2 H, ArNHN(m)), 9.43 (s, 0.8 H, $CSNH_2$(M)), 9.55 (s, 0.8 H, $CSNH_2$(M)), 11.14 (s, 0.8 H, ArNNH(M)). ^{13}C NMR (400 MHz, DMSO-d_6, 300 K): δ(ppm) = 12.5 (CH_3, SMe(m)), 13.2 (CH_3, SMe(M)), 55.34 (CH_3, OMe), 114.5

(7) Whalen, A. K.; Bhattacharya, S.; Pierpont, C. G. *Inorg. Chem.* **1994**, *33*, 347.
(8) Hazell, R. G. *Acta Chem. Scand.* **1976**, *A30*, 322.
(9) Jensen, K. A.; Bechgaard, K.; Pedersen, C. T. *Acta Chem. Scand.* **1972**, *26*, 2913.
(10) Pilgram, K. H. *Synth. Comm.* **1985**, *15*, 697.
(11) Pyl, T.; Scheel, K. H.; Beyer, H. *J. Prakt. Chem.* **1963**, *4(20)*, 255.

(CH, *m*-ArNN(M)), 114.8 (CH, *m*-ArNN(m)), 115.1 (CH, *o*-ArNN), 139.5 (Cq, ArNN), 154.2 (Cq, *p*-ArNN), 170.3 (Cq, C(SMe)(M)), 176.5 (Cq, C(SMe)(m)).

***S*-Methyl-1-phenyl-4-phenyl-isothiosemicarbazide Hydroiodide, $H_2[L^4]$·HI.** The starting material 1-phenyl-4-phenyl-isothiosemicarbazide was synthesized by using a slight modification of a published procedure.[12] Phenylhydrazine hydrochloride (7.2 g, 50 mmol) was suspended in 20 mL of absolute ethanol. Phenylisothiocyanate (6.8 g, i.e., 6.0 mL, 50 mmol) and pyridine (5 mL) were added. The slurry was heated to reflux for 2 h. After cooling of the mixture to 20 °C, distilled water (5 mL) was added. The white precipitate was filtered off, washed twice with ethanol (5 mL), and dried under vacuum to yield 8.73 g of 1-phenyl-4-phenyl-isothiosemicarbazide (72%). EI-MS: $m/z = 243$ for $\{C_{13}H_{13}N_3S\}^+$. ^{1}H NMR (500 MHz, DMSO-d_6, 300 K): δ(ppm) = 6.79 (d, J = 8 Hz, 2H, *o*-ArNN), 6.83 (d, J = 7.5 Hz, 1 H, *p*-ArNN), 7.12 (t, J = 7.5 H, 1H, *p*-ArNC), 7.23 (t, J = 8 Hz, 2H, *m*-ArNN), 7.29 (t, J = 7.5 Hz, 2H, *m*-ArNC), 7.55 (d, J = 8 Hz, 2H, *o*-ArNC), 8.08 (br, s, 1H, NH), 9.70 (s, 1H, NH), 9.82 (br, s, 1H, NH). ^{13}C NMR (500 MHz, DMSO-d_6, 300 K): δ(ppm) = 113.0 (CH, *o*-ArNN), 119.8 (CH, *p*-ArNN), 124.7 (CH, *p*-ArNC), 125.0 (CH, *o*-ArNC), 127.9 (CH, *m*-ArNC), 128.8 (CH, *m*-ArNN), 139.2 (Cq, ArNC), 148.0 (Cq, ArNN), 181.1 (Cq-CS). To 1-phenyl-4-phenyl-isothiosemicarbazide (3 g, 12.3 mmol) suspended in 50 mL absolute ethanol was added methyl iodide (1.75 g, 0.77 mL, 12.3 mmol). The mixture was heated to reflux for 2 h yielding a pale yellow solution, which was cooled to 20 °C. The solvent ethanol was removed by evaporation. Yield: 4.87 g of yellow oily *S*-methyl-1-phenyl-4-phenyl-isothiosemicarbazide hydroiodide, which was used without further purification. EI-MS: m/z = 257 for $\{C_{14}H_{15}N_3S\}^+$. By analogy with the former cases, the ^{1}H NMR (400 MHz, CD_3OD, 300 K) spectrum shows the presence of two tautomers in equilibrium at 300 K in a 7:3 ratio; δ(ppm) = 2.74 and 2.75 (s, SMe), 6.94 (d, J = 8.4 Hz and t), 7.05 (t, J = 7.4 Hz), 7.13 (d, J = 7.8 Hz), 7.30 (t, J = 7.8 Hz), 7.37−7.57 (m), 7.59−7.65 (m). ^{13}C NMR (400 MHz, CD_3OD, 300 K): δ(ppm = 14.4 and 14.7 (SMe), 114.7, 115.2, 122.8, 123.1, 127.7, 128.2, 130.18, 130.23, 130.3, 130.5, 130.7, 131.5, 135.5, 135.7, 146.6, 172.9 and 177.1 (Cq-S).

***S*-Methyl-1-*p*-methoxyphenyl-4-phenyl-isothiosemicarbazide Hydroiodide, $H_2[L^6]$·HI.** The same procedure as for $H_2[L^4]$·HI was applied starting with *p*-methoxyphenylhydrazine hydrochloride (5 g, 28.6 mmol) and phenyl isothiocyanate (3.87 g, i.e., 3.4 mL, 28.6 mmol). A total of 6.28 g of 1-*p*-methoxyphenyl-4-phenyl-isothiosemicarbazide was isolated as a white powder (Yield 80%). EI-MS: $m/z = 273$ for $\{C_{14}H_{15}N_3OS\}^+$. ^{1}H NMR (500 MHz, DMSO-d_6, 300 K): δ(ppm) = 3.67 (s, 3H, MeO), 6.73 (d, J = 8.5 Hz, 2H, *o*-ArNN), 6.84 (d, J = 8.5 Hz, 2H, *m*-ArNN), 7.11 (t, J = 7.5 Hz, 1H, *p*-ArNC Hz, 2H, *o*-ArNC), 7.77 (br s, 1H, NH), 9.65 (s, 1H, NH), 9.79 (s, 1H, NH). ^{13}C NMR (500 MHz, DMSO-d_6, 300 K): δ(ppm) = 55.3 (CH_3, OMe), 114.3 (CH, *m*-ArNN), 114.5 (CH, *o*-ArNN), 124.5 (CH, *p*-ArNC), 124.8 (CH, *o*-ArNC), 127.8 (CH, *m*-ArNC), 139.1 (Cq, ArNC), 141.5 (CQ, ArNN), 153.5 (Cq, MeOAr), 180.8 (Cq, CS). The methylation was performed on 3 g of 1-*p*-methoxyphenyl-4-phenyl-isothiosemicarbazide (11.0 mmol) with 1.55 g methyl iodide (0.68 mL, 11.0 mmol). Evaporation of the ethanol solvent and precipitation in dichloromethane at −30 °C yielded 4.29 g of *S*-methyl-1-*p*-methoxyphenyl-4-phenyl-isothiosemicarbazide hydroiodide as a white powder (Yield: 95%). EI-Ms: $m/z = 287$ for $\{C_{15}H_{17}N_3OS\}^+$. ^{1}H NMR (400 MHz, CD_3OD, 300 K) (By analogy with the former cases, two conformers in equilibrium at 300 K in a 2:1 ratio): δ(ppm) = 2.68 and 2.70 (s, SMe), 3.72 and 3.76 (OMe), 6.84 (br s), 6.94 (d, J = 8.8 Hz), 7.02 (d, J = 8.8 Hz), 7.39 (d, J = 7.4 Hz), 7.42−7.60 (m). ^{13}C NMR (400 MHz, CD_3OD, 300 K): δ(ppm) = 14.0 and 14.2 (SMe), 56.1 (OMe), 115.7, 115.9, 116.6, 117.2, 127.8, 128.4, 130.3, 130.6, 130.8, 131.6, 136.0, 140.2, 156.8, 157.0, 172.9 and 177.2 (Cq-S).

***S*-Methyl-1-*p*-nitrophenyl-4-phenyl-isothiosemicarbazide Hydroiodide, $H_2[L^5]$·HI.** The same procedure as for $H_2[L^4]$·HI was applied starting with *p*-nitrophenylhydrazine hydrochloride (1.89 g, 10 mmol) and phenyl isothiocyanate (1.35 g, i.e., 1.2 mL, 10 mmol). 2.61 g of 1-*p*-nitrophenyl-4-phenyl-isothiosemicarbazide was isolated as a pale yellow powder (Yield 90%). EI-MS: m/z = 288 for $\{C_{13}H_{12}N_4O_2S\}^+$. ^{1}H NMR (500 MHz, DMSO-d_6, 300 K): δ(ppm) = 6.82 (d, J = 9 Hz, *o*-ArNN), 7.14 (t, J = 7.3 Hz, 1H, *p*-ArNC), 7.30 (t, J = 7.3 Hz, 2H, *m*-ArNC), 7.45 (d, J = 7.3 Hz, 2H, *o*-ArNC), 8.14 (d, J = 9 Hz, 2H, *m*-ArNN), 9.19 (s, 1H, NH), 9.90 (br s, 1H, NH), 9.95 (br, s, 1H, NH). ^{13}C NMR (500 MHz, DMSO-d_6, 300 K): δ(ppm) = 111.6 (CH, *m*-ArNN), 125.1 (CH, *p*-ArNC), 125.7 (CH, *o*-ArNC), 125.8 (CH, *m*-ArNN), 128.0 (CH, *m*-ArNC), 139.1 (Cq, ArNC and NO_2Ar), 154.1 (Cq, ArNN), 181.5 (Cq, CS). The methylation was performed on 2.5 g of 1-*p*-nitrophenyl-4-phenyl-isothiosemicarbazide (8.7 mmol) with 1.36 g methyl iodide (0.59 mL, 9.5 mmol). Evaporation of the ethanol solution yielded 3 g of dark red oily *S*-methyl-1-*p*-nitrophenyl-4-phenyl-isothiosemicarbazide, which was used without further purification. EI-MS: m/z = 302 for $\{C_{14}H_{14}N_4O_2S\}^+$. ^{1}H NMR (250 MHz, DMSO-d_6, 300 K): δ(ppm) = 2.67 (s, 3H, SMe), 6.85−7.00 (m, 3H), 7.24−7.34 (m, 3H), 7.40−7.51 (m, 4H), 8.55 (s, br, NH). ^{13}C NMR (400 MHz, DMSO-d_6, 300 K): δ(ppm) = 13.92 (CH_3), 111.4, 111.5, 125.4, 125.6, 127.0, 127.8, 128.9, 138.4, 151.4.

$[Ni^{II}(L^{1\bullet})_2]$ (1).[1] This complex was synthesized using a slight modification of the literature procedure.[1] To a pale yellow solution of *S*-methyl-1-phenylisothiosemicarbazide hydroiodide (2 g, 6.36 mmol) in ethanol (40 mL) was added $Ni(OAc)_2$·$4H_2O$ (793 mg, 3.18 mmol) in the presence of air. Upon addition of Et_3N (2.65 mL, 19.1 mmol), a darkening of the solution occurred. After 2 h of stirring at room temperature, a dark green precipitate was filtered off and washed with ethanol to yield 880 mg of **1** (66% yield). X-ray quality crystals were grown by slow evaporation of the solvent from a concentrated solution of **1** in ethyl acetate. ^{1}H NMR (400 MHz, $CDCl_3$, 300 K): δ(ppm) = 2.45 (s, 6H, SCH_3), 5.86 (br s, 2H, NH), 7.43 (m, 6H, *m*-ArH and *p*-ArH), 7.97 (d of m, 4H, ^3J = 6.8 Hz, *o*-ArH). ^{13}C NMR (400 MHz, $CDCl_3$, 300 K): δ(ppm) = 15.7 (CH_3, SMe), 125.0 (CH, *o*-Ar), 127.0 (CH, *p*-Ar), 129.3 (CH, *m*-Ar), 156.2 (C_q, Ar), 164.5 (C_q, CSMe).

$[Ni^{II}(L^{2\bullet})_2]$ (2). The same procedure as described for **1** was used by starting with S-methyl-1-*p*-nitrophenyl-isothiosemicarbazide hydroiodide, $H_2[L^2]$·HI, (708 mg, 2 mmol) to yield 470 mg (92%) of dark red crystalline **2**. EI-MS: m/z = 506 for $\{C_{16}H_{16}N_8NiS_2\}^+$. Anal. Calcd for $C_{16}H_{16}N_8NiS_2$: C, 37.89; H, 3.18; N, 22.09; Ni, 11.57. Found: C, 38.04; H, 3.24; N, 21.91; Ni, 11.53. ^{1}H NMR (400 MHz, $CDCl_3$, 300 K): δ(ppm) = 2.51 (s, 6H, SCH_3), 5.99 (br s, 2H, NH), 8.16 (d, 4H, J = 9.2 Hz, HAr), 8.29 (d, 4H, J = 9.2 Hz, HAr).

$[Ni^{II}(L^{3\bullet})_2]$ (3). The same procedure as described for **1** was used by starting with *S*-methyl-1-*p*-methoxyphenyl-isothiosemicarbazide hydroiodide, $H_2[L^3]$·HI, (820 mg, 2.5 mmol) to yield 490 mg (82%) of dark red microcrystalline **3**. EI-MS: m/z = 476 for $\{C_{18}H_{22}N_6NiO_2S_2\}^+$. Anal. Calcd for $C_{18}H_{22}N_6NiO_2S_2$: C, 45.30; H, 4.65; N, 17.61; Ni, 12.30. Found: C, 45.38; H, 4.63; N, 17.59; Ni, 12.32. ^{1}H NMR (400 MHz, $CDCl_3$, 300 K): δ(ppm) = 2.44 (s, 6H, SCH_3), 3.87 (s, 6H, OCH_3), 5.85 (br s, 2H, NH), 6.95 (d, 4H, J = 9.0 Hz, *m*-HArNN), 8.03 (d, 4H, J = 9.0 Hz, *o*-HArNN).

(12) Wu, M. T.; Waksmunski, F. S.; Hof, D. R.; Fisher, M. H.; Egerton, J. R.; Patchett, A. A. *J. Pharm. Sci.* **1977**, *66*, 1150.

$[Ni^{II}(L^{4\bullet})_2]$ (4).[1b] The same procedure as for **1** was used by starting with *S*-methyl-1-phenyl-4-phenyl-isothiosemicarbazide hydroiodide, $H_2[L^4]\cdot HI$, (1.5 g, 3.9 mmol) to yield 880 mg (79%) of dark red crystalline **4**. EI-MS: $m/z = 568$ for $\{C_{28}H_{26}N_6NiS_2\}^+$. Anal. Calcd for $C_{28}H_{26}N_6NiS_2$: C, 59.07; H, 4.60; N, 14.76; Ni, 10.31. Found: C, 58.88; H, 4.76; N, 14.67; Ni, 10.32. ^{1}H NMR (500 MHz, $CDCl_3$, 300 K): δ(ppm) = 2.30 (s, 6H, SCH_3), 7.03 (t, 4H, $J = 7.8$ Hz, *m*-HArNN), 7.22 (d, 2H, $J = 7.4$ Hz, *p*-HArNC), 7.29 (t, 4H, $J = 7.6$ Hz, *m*-HArNC), 7.50 (d, 4H, $J = 7.1$ Hz, *o*-HArNC), 7.95 (t, 2H, $J = 7.4$ Hz, *p*-HArNN), 9.52 (d, 4H, $J = 8.1$ Hz, *o*-HArNN). ^{13}C NMR (400 MHz, $CDCl_3$, 300 K): δ(ppm) = 15.3 (CH_3, SMe), 120.0 (CH, *o*-ArNN), 122.8 (CH, *p*-ArNN), 123.8 (CH, *o*-ArNC), 125.9 (CH, *p*-ArNC), 128.7 (CH, *m*-ArNC), 133.8 (CH, *m*-ArNN), 151.9 (C_q, ARNC), 157.2 (C_q, CSMe), 167.3 (C_q, ArNN).

$[Ni^{II}(L^{5\bullet})_2]$ (5).[3] The same procedure as for **1** was used by starting with *S*-methyl-1-*p*-nitrophenyl-4-phenyl-isothiosemicarbazide hydroiodide, $H_2[L^5]\cdot HI$, (1.5 g, 3.5 mmol) to yield 930 mg (80%) of dark red crystalline **5**. X-ray quality crystals were grown from a concentrated solution of **5** in ethyl acetate by slow evaporation of the solvent. EI-MS: $m/z = 658$ for $\{C_{28}H_{24}N_8NiO_4S_2\}^+$. Anal. Calcd for $C_{28}H_{24}N_8NiO_4S_2$: C, 51.00; H, 3.67; N, 16.99; Ni, 8.90. Found: C, 50.81; H, 3.76; N, 17.11; Ni, 9.14. ^{1}H NMR (400 MHz, $CDCl_3$, 300 K): δ(ppm) = 2.34 (s, 6H, SCH_3), 7.31 (m, 6H, *m*-HArNC and *p*-HArNC), 7.53 (m, 4H, *o*-HArNC), 7.91 (ABA′ pattern, $^3J = 9.2$ Hz, $^4J = 2.68$ Hz, *m*-HArNN), 9.52 (ABA′ pattern, $^3J = 9.2$ Hz, $^4J = 2.68$ Hz, *o*-HArNN). ^{13}C NMR (400 MHz, $CDCl_3$, 300 K): δ(ppm) = 15.6 (CH_3, SMe), 120.6 (CH, *o*-ArNN), 123.5 (CH, *o*-ArNC), 126.8 (CH, *p*-ArNC), 129.1 (CH, *m*-ArNC), 129.6 (CH, *p*-ArNN), 140.3 (C_q, *p*-ArNN), 151.3 (C_q, ArNC), 162.1 (C_q, CSMe), 170.7 (C_q, ArNN).

$[Ni^{II}(L^{6\bullet})_2]\cdot 0.5H_2O$ (6). The same procedure as described for **1** was used by starting with *S*-methyl-1-*p*-methoxyphenyl-4-phenyl-isothiosemicarbazide hydroiodide, $H_2[L^6]\cdot HI$, (1.5 g, 3.6 mmol) to yield 880 mg (79%) of dark red crystalline **6**. X-ray quality crystals were grown by slow evaporation of the solvent from a concentrated solution of **6** in ethyl acetate. EI-MS: $m/z = 628$ for $\{C_{30}H_{30}N_6NiO_2S_2\}^+$ $\{[Ni(L_{Ph}{}^{MeO*})_2]^+\}$. Anal. Calcd for $C_{30}H_{31}N_6NiO_{2.5}S_2$: C, 56.44; H, 4.89; N, 13.16; Ni, 9.19. Found: C, 56.42; H, 4.76; N, 13.13; Ni, 9.28. ^{1}H NMR (400 MHz, $CDCl_3$, 300 K): δ(ppm) = 2.26 (s, 6H, SCH_3), 6.61 (d, 4H, $J = 8.2$ Hz, *m*-HArNN), 7.22 (t, 2H, $J = 7.1$ Hz, *p*-HArNC), 7.29 (t, 4H, $J = 7.6$ Hz, *m*-HArNC), 7.48 (d, 4H, $J = 7.4$ Hz, *o*-HArNC), 9.57 (d, 4H, $J = 8.8$ Hz, *o*-HArNN). ^{13}C NMR (400 MHz, $CDCl_3$, 300 K): δ(ppm) = 15.2 (CH_3, SMe), 55.5 (CH_3, OMe), 119.3 (CH, *m*-ArNN), 121.3 (CH, *o*-ArNN), 124.1 (CH, *o*-ArNC), 125.6 (CH, *p*-ArNC), 128.6 (CH, *m*-ArNC), 151.9 (C_q, ArNC), 154.4 (C_q, ArNN), 155.4 (C_q, CSMe), 162.4 (C_q, ArNN).

$[Ni^{II}(L^{1,ox})_2I_2]\cdot 2CHCl_3$ (7·2CHCl$_3$).[2] To a green solution of **1** (230 mg, 0.55 mmol) in chloroform (6 mL) at 40 °C was added dropwise a solution of I_2 (140 mg, 0.55 mmol) in chloroform (3 mL). The color of the solution changed to brownish. It was then cooled to 25 °C. The crystalline material was filtered off. Yield: 445 mg. Anal. Calcd for $C_{18}H_{20}Cl_6I_2N_6NiS_2$: C, 23.76; H, 2.22; N, 9.24; Ni, 6.45; I, 27.9. Found: C, 23.75; H, 2.14; N, 9.31; Ni, 6.35; I, 27.52. X-ray quality crystals of unsolvated $[Ni(L^{ox})_2I_2]$ (**7**) were obtained by slow evaporation of the solvent from a 1/3 toluene and 2/3 dichloromethane solution.

$[Ni^{II}(L^{1,ox})_3](I_3)_2$ (8). An X-ray quality single crystal of **8** was obtained from slow evaporation of the solvent from the crude filtrate obtained upon synthesis of solvated **7** (see above). Every attempt to synthesize this molecule in a rational fashion has been unsuccessful.

***trans*-$[Ni^{II}(L^{5,ox})_2(I_3)_2]\cdot 2CHCl_3$ (9·2CHCl$_3$).** To a purple solution of **5** (132 mg; 0.2 mmol) in $CHCl_3$ (5 mL) was added at 40 °C a solution of I_2 (155 mg; 0.6 mmol) in $CHCl_3$ (30 mL) with stirring. The color of the solution turned brownish. After 20 min the solution was allowed to cool to 20 °C and the $CHCl_3$ was allowed to slowly evaporate. X-ray quality of brown-black crystals of **9**·2$CHCl_3$ were obtained (280 mg, 80% yield). Anal. Calcd for $C_{30.3}H_{26.3}Cl_{6.9}I_{6.4}N_8NiO_4S_2$ (9·(2.3$CHCl_3$)·(0.2I_2)):C, 20.84; H, 1.52; N, 6.42; Ni, 3.36; I, 46.51. Found: C, 20.66; H, 1.45; N, 6.59; Ni, 3.43; I, 46.58.

($L^{6,ox}$) (10). Solid **6** (315 mg, 0.5 mmol) was dissolved in chloroform (10 mL) and heated to 40 °C. Then a solution of I_2 (127 mg, 0.5 mmol) in chloroform (20 mL) was added dropwise. The initially red purple solution rapidly turned brownish. It was taken to dryness, redissolved in dichloromethane (5 mL), and pentane (20 mL) was added. A brown precipitate was filtered off, and the filtrate was left for slow evaporation to yield 80 mg (28%) of X-ray quality reddish crystals of ($L^{6,ox}$) (**10**). EI-MS: $m/z = 285$ for $\{C_{15}H_{15}N_3OS\}^+$. Anal. Calcd for $C_{15}H_{15.4}N_3O_{1.2}S$ ($(L^{ox}{}_{Ph}{}^{MeO})\cdot 0.2(H_2O)$): C, 62.35; H, 5.37; N, 14.54. Found: C, 62.45; H, 5.47; N, 14.39. ^{1}H NMR (400 MHz, $CDCl_3$, 300 K): δ(ppm) = 2.49 (s, 3H, SMe), 3.86 (s, 3H, OMe), 6.93 (d, 2H, $J = 8.8$ Hz, *m*-HArNN), 7.04 (d, 2H, $J = 7.6$ Hz, *o*-HArNC), 7.12 (t, 1H, $J = 7.6$ Hz, *p*-HArNC), 7.30 (t, 2H, $J = 7.6$ Hz, *m*-HArNC), 7.75 (d, 2H, $J = 8.8$ Hz, *o*-ArNN). ^{13}C NMR (400 MHz, $CDCl_3$, 300 K): δ(ppm) = 13.8 (CH_3, SMe), 55.7 (CH_3, OMe), 114.5 (CH, *m*-ArNN), 123.2 (CH, *o*-ArNC), 124.3 (*p*-ArNC), 126.6 (CH, *o*-ArNN), 128.2 (CH, *m*-ArNC), 145.9 (C_q, ArNN), 148.1 (C_q, ArNC), 164.1 (C_q, *p*-ArNN), 166.0 (C_q, CSMe).

3-Methylsulfanyl-1-(4-nitrophenyl)-1,4-dihydrobenzo[1,2,4]-triazine (11). This compound was isolated in an attempt to synthesize the zinc complex $[Zn(L^{5\bullet})_2]$: To a suspension of $H_2[L^5]\cdot HI$ (430 mg, 1 mmol) in ethanol (10 mL), $Zn(OAc)_2\cdot 2H_2O$ (110 mg, 0.5 mmol) and triethylamine (140 μL, 1 mmol) were added. Upon stirring of the sample in the air, a dark color quickly developed. After 10 min of stirring, 2 more equivalents of triethylamine (280 μL, 2 mmol) were added and the mixture was stirred for an additional 2 h. Upon concentration of the solution by slow evaporation (2 days) of the solvent ethanol a dark microcrystalline material formed, which was filtered off yielding 160 mg of **11** (53% yield). Slow evaporation of a concentrated dichloromethane solution afforded X-ray quality single crystals. EI-MS: $m/z = 300$ for $\{\mathbf{11}\}^+$ ($C_{14}H_{12}N_4O_2S$). ^{1}H NMR (400 MHz, DMSO-d_6, 300 K): δ(ppm) = 2.52 (s, 3H, SMe), 6.80 (d, 1H, $J = 7.6$ Hz, *o*-$H_{benzotriazine}$), 7.00 (m, 2H, *m*-$H_{benzotriazine}$ and *m*′−$H_{benzotriazine}$), 7.19 (d, 1H, $J = 7.8$ Hz, *o*′-$H_{benzotriazine}$), 7.46 (d, 2H, $J = 8$ Hz, *o*-HArNN), 8.11 (d, 2H, $J = 8$ Hz, *m*-HArNN), 9.75 (s, 1H, NH). ^{13}C NMR (400 MHz, $CDCl_3$, 300 K): δ(ppm) = 13.4 (CH_3, SMe), 112.8 (CH, *o*-ArNN), 114.6 (CH, *o*-$Ar_{benzotriazine}$), 116.5 (CH, *o*′-$Ar_{benzotriazine}$), 123.3 (CH, *m*′-$H_{benzotriazine}$), 125.5 (CH, *m*-ArNN), 125.7 (*m*-$Ar_{benzotriazine}$), 127.6 (C_q, $Ar_{benzotriazine}$), 134.5 (C_q, $Ar_{benzotriazine}$), 138.3 (C_q, $ArNO_2$), 148 (C_q, ArNN), 156.3 (C_q, CSMe).

X-ray Crystallographic Data Collection and Refinement of the Structures. A dark green single crystal of **1**, dark red crystals of **5**, **7**, **9**, **10** and **11**, and black crystals of **6** and **8** were coated with perfluoropolyether and mounted in the nitrogen cold stream of a Nonius Kappa-CCD diffractometer equipped with a Mo-target rotating-anode X-ray source and a graphite monochromator (Mo−Kα, $\lambda = 0.71073$ Å). Final cell constants were obtained from least-squares fits of a subsets of several thousand strong reflections. Data collections were performed by taking frames at 1.0° in ω (0.8° in case of **8**, 1.5° for **11**). Crystal faces of **1** and **6**−**9** were determined, and the corresponding intensity data were corrected for absorption using the Gaussian-type routine embedded in XPREP.[13] Data sets

Table 1. Crystallographic Data for **1** and **5**−**11**

	1	**5**	**6**	**7**
chem formula	$C_{16}H_{18}N_6NiS_2$	$C_{28}H_{24}N_8NiO_4S_2$	$C_{30}H_{30}N_6NiO_2S_2$	$C_{16}H_{18}I_2N_6NiS_2$
fw	417.19	659.38	629.43	670.99
space group	$P\bar{1}$, No. 2	$P2_1/c$, No. 14	*Pbcn*, No. 60	$P2_1/c$, No. 14
a, Å	9.9844(3)	11.4764(4)	11.8076(4)	8.6347(3)
b, Å	10.0508(3)	19.1692(6)	13.7892(4)	14.3456(5)
c, Å	10.2507(3)	13.0665(4)	17.6810(6)	9.4459(4)
α, deg	81.478(6)	90	90	90
β, deg	62.793(6)	91.62(1)	90	111.467(4)
γ, deg	89.716(6)	90	90	90
V, Å	902.45(5)	2873.4(2)	2878.8(2)	1088.89(7)
Z	2	4	4	2
T, K	100(2)	100(2)	100(2)	100(2)
ρ calcd, g cm^{-3}	1.535	1.524	1.452	2.047
reflns collected/$2\Theta_{max}$	27647/61.9	74991/62.0	40004/62.08	28577/61.92
unique reflns/$I > 2\sigma(I)$	5661/5338	9116/8256	4604/3571	3444/3210
no. of params/restr	235/1	390/0	188/0	129/0
μ(Mo Kα), cm^{-1}	13.18	8.76	8.59	39.32
R1[a] goodness of fit [b]	0.0231/1.057	0.0282/1.047	0.0399/1.038	0.0148/1.105
wR2[c] ($I > 2\sigma(I)$)	0.0550	0.0655	0.0748	0.0340
residual density, eÅ^{-3}	+0.45/−0.37	+0.39/−0.25	+0.42/−0.43	+0.53/−0.40

	8	**9**	**10**	**11**
chem formula	$C_{24}H_{27}I_6N_9NiS_3$	$C_{30}H_{26}Cl_6I_6N_8NiO_4S_2$	$C_{15}H_{15}N_3OS$	$C_{14}H_{12}N_4O_2S$
Fw	1357.84	1659.52	285.36	300.34
space group	*Pbca*, No. 61	$P\bar{1}$, No. 2	*Pn*, No. 7	$P2_1/c$, No. 14
a, Å	15.5006(6)	9.7733(6)	11.8164(6)	14.9324(10)
b, Å	16.9618(6)	11.4035(6)	9.8640(4)	11.9210(8)
c, Å	29.2707(10)	11.5154(8)	24.5392(12)	7.4166(6)
α, deg	90	71.14(1)	90	90
β, deg	90	75.65(1)	91.97(1)	95.02(1)
γ, deg	90	76.89(1)	90	90
V, Å	7695.8(5)	1161.43(12)	2858.5(2)	1315.2(2)
Z	8	1	8	4
T, K	100(2)	100(2)	100(2)	100(2)
ρ calcd, g cm^{-3}	2.344	2.373	1.326	1.517
reflns collected/$2\Theta_{max}$	41986/60.0	27801/62.04	28776/52.0	20117/60.0
unique reflns/$I > 2\sigma(I)$	11158/8578	7381/7069	11006/8597	3825/2907
no. of params/restr.	401/0	290/30	722/2	190/0
μ(Mo Kα), cm^{-1}	55.11	48.84	2.25	2.57
R1[a]/ goodness of fit[b]	0.0488/1.016	0.0291/1.096	0.0609/1.019	0.0482/1.019
wR2[c] ($I > 2\sigma(I)$)	0.1088	0.0666	0.1106	0.0949
residual density, eÅ^{-3}	+2.36/−3.35	+3.29/−2.46	+0.62/−0.34	+0.37/−0.34

[a] Observation criterion: $I > 2\sigma(I)$. $R1 = \sum||F_o| - |F_c||/\sum|F_o|$. [b] GOF $= [\sum[w(F_o^2 - F_c^2)^2]/(n-p)]^{1/2}$. [c] $wR2 = [\sum[w(F_o^2 - F_c^2)^2]/\sum[w(F_o^2)^2]]^{1/2}$ where $w = 1/\sigma^2(F_o^2) + (aP)^2 + bP$, $P = (F_o^2 + 2F_c^2)/3$.

5, **10**, and **11** were not corrected for absorption. Crystallographic data of the compounds are listed in Table 1. The Siemens ShelXTL[13] software package was used for solution and artwork of the structure, and ShelXL97[14] was used for the refinement. The structures were readily solved by direct and Patterson methods and subsequent difference Fourier techniques. All non-hydrogen atoms were refined anisotropically. Hydrogen atoms attached to carbon atoms were placed at calculated positions and refined as riding atoms with isotropic displacement parameters. Protons bound to nitrogen atoms in **1**, **7** and **8** were located from the difference map and refined with restrained bond distances (ShelX SADI instruction) and thermal parameters. One of the two I_3^- anions in **8** was found to be disordered. Two positions in a 91:9 ratio were refined with equal thermal parameters of corresponding I-atoms (ShelX EADP instruction). Structure of **10** was first thought to be centrosymmetric (space group $P2_1/n$), but disorder problems led to the conclusion that the structure is more accurately described in space group *Pn*. The "disorder problems" vanished completely refining four independent molecules, one of them having a different conformation of the methoxy group. The chloroform molecule in the asymmetric unit of **9** is disordered. Two split positions were refined with constrained C−Cl and Cl−Cl distances. A total of 30 constraints was used, but residual electron density suggests that the disorder of the molecule, residing in a I_3^- walled solvent channel, is even more complicated, but a third split position could not be refined yielding a stable solution.

Physical Measurements. Electronic spectra of complexes and corresponding spectra from spectroelectrochemical measurements were recorded on an HP 8452 A diode array spectrophotometer (range: 200−1700 nm). Cyclic voltammograms and coulometric experiments were performed with an EG & G potentiostat/galvanostat. Variable field (1−7 T), variable temperature (4−300 K) magnetization data were recorded on a SQUID magnetometer (MPMS Quantum Design). The experimental magnetic susceptibility data were corrected for underlying diamagnetism by use of tabulated Pascal's constants. X-band EPR spectra were recorded on a Bruker ESP 300 spectrometer.

Calculations. All calculations reported in this paper were done with the program package ORCA.[15] As will be further discussed in the text, the geometry optimizations were carried out at the BP86 and B3LYP levels of DFT.[16] These functionals have proved in many applications their ability to reliably predict structures of transition

(13) *ShelXTL V.5*, Siemens Analytical X-ray Instruments, Inc.; Madison, WI, 1994.
(14) Sheldrick, G. M. *ShelXL97*; University of Göttingen, 1997.

metal complexes. However, in the present case they yield distinctly different results, which made a comparison of both approaches necessary. The all-electron Gaussian basis sets used were those reported by the Ahlrichs group.[17] Accurate triple-ξ valence basis sets with one set of polarization functions on the all atoms were used (TZV(P)). The auxiliary basis sets used to fit the electron density were taken from the Turbomole library (Basis sets were obtained from the ftp server of the quantum chemistry group at the university of Karlsruhe (Germany) under ftp://ftp.chemie.uni-karlsruhe.de/pub/basen/) and were chosen to match the orbital basis.

The SCF calculations were always of the spin-polarized type and were tightly converged (10^{-7} Eh in energy, 10^{-6} Eh in the density change and 10^{-6} in maximum element of the DIIS error vector). Single point calculations with the B3LYP functional were carried out at the optimized geometries to predict EPR and absorption spectral parameters. In the calculation of the EPR, the same basis sets were used as in the geometry optimization, except for the metal basis which was the triply polarized "Core Properties" (CP(PPP)) basis.[18a] Ab initio calculations of the optical spectra were also undertaken with the ORCA program and utilized the recently developed spectroscopy oriented configuration interaction (SORCI) formalism.[18b] The calculations were started from closed-shell B3LYP orbitals and the thresholds used were $T_{sel} = 10^{-6}$ Eh, $T_{pre} = 10^{-2}$, and $T_{nat} = 10^{-5}$. The basis set used in the SORCI calculation was reasonably large and based on Ahlrichs's triple-ζ basis augmented with 2p and 1f polarization functions on the central nickel, two sets of d-functions on C,N and S and one set of p-functions on H, all taken from the TurboMole library (see above).

Results

Synthesis of Ligands and Complexes. To evaluate the influence of electronic and steric effects on the structure of their nickel complexes, we used the two series of ligands shown in Scheme 1: on one hand, the *S*-methyl-1-phenyl-isothiosemicarbazide series $H_2[L^{1-3}]$ with *p*-phenyl substituents H, NO_2, OCH_3, and, on the other hand, the bulkier 1,4-diphenyl series $H_2[L^{4-6}]$ where the 1-phenyl group again carries an H, NO_2, or OCH_3 substituent in the para-position.

The corresponding neutral, highly colored bis(ligand)-nickel(II) complexes **1**−**6** (Scheme 3) were synthesized by reaction of 2 equiv of the respective ligand $H_2[L^{1-6}]\cdot HI$ dissolved in ethanol in the presence of excess triethylamine and air with 1 equiv of $[Ni^{II}(CH_3CO_2)_2]\cdot 4H_2O$. Dark precipitates of microcrystalline powders were obtained in good to excellent yields. The EI mass spectra of **1**−**6** each display a molecular ion peak $\{M\}^+$ in agreement with their formulation as $[Ni^{II}(L^{1-6\bullet})_2]$. Complexes **1** and **5** have been prepared previously.[1,3] Species **1**−**6** are diamagnetic (S = 0) as was judged from their ^1H NMR spectra and magnetic susceptibility measurements (see below). Complexes **1**−**3** exhibit a single ν(N−H) stretching frequency at 3354 cm^{-1} for **1**, 3368 cm^{-1} for **2**, and 3371 cm^{-1} for **3**. In contrast, complexes **4**−**6** do not display this mode.

Oxidation of square planar **1** with iodine in chloroform yields octahedral *trans*-$[Ni(L^{1,ox})_2I_2]\cdot 2CHCl_3$ (**7**·2$CHCl_3$).[2] In one instance, using the conditions given in the experimental section for the synthesis of **7**, we obtained single crystals of octahedral $[Ni^{II}(L^{1,ox})_3](I_3)_2$ (**8**). The preparation of **8** is as yet not rationally reproducible. Temperature-dependent magnetic susceptibility measurements on a solid sample of **7**·2$CHCl_3$ in an external magnetic field of 1.0 T revealed that the molecular species possesses an S = 1 ground state. From the fit of the data of additional measurements at 4 and 7 T shown in Figure S1 (Supporting Information) the following spin Hamiltonian parameters for **7** were obtained: S = 1; $g_{iso} = 2.14$ (±0.02), $|D| = 4.0 \pm 1$ cm^{-1}.

Note that when a 3-fold excess of iodine was used for the oxidation, the octahedral *trans*-$[Ni^{II}(L^{1,ox})_2(I_3)_2]$ was isolated.[2] Oxidation of tetrahedral $[Ni^{II}(L^{5\bullet})_2]$ with an equivalent of iodine resulted in the isolation in ca. 30% yield of *trans*-$[Ni^{II}(L^{5,ox})_2(I_3)_2]$ (**9**). Using a 3-fold excess iodine, the yield was improved to 80% of isolated **9**. The strong electron withdrawing NO_2 group probably renders the $(L^{5\bullet})^-$ anion harder to oxidize, thus favoring formation of coordinated $(I_3)^-$ anions over the oxidation of another $[Ni(L^{5\bullet})_2]$ molecule. Fitting of temperature-dependent magnetic susceptibility measurements on a solid sample of **9**·2$HCCl_3$ (Figure S2, Supporting Information) in external fields of 1, 4, and 7 T revealed that the molecule possesses an S = 1 ground state and leads to the following spin Hamiltonian parameters: $g_{iso} = 2.08$ and $|D| = 6.0 \pm 0.5$ cm^{-1}.

Oxidation of tetrahedral $[Ni^{II}(L^{6\bullet})_2]$ (**6**) with iodine in chloroform affords red single crystals of the metal free, oxidized ligand $(L^{6,ox})^0$ (**10**) in 28% yield (Scheme 4). Attempts to prepare this molecule directly from $H_2[L^6]\cdot HI$ by oxidation with I_2 led to complicated mixtures of organic compounds, which we did not investigate further.

An attempt to synthesize the analogous tetrahedral zinc complexes $[Zn(L^{6\bullet})_2]$ and $[Zn(L^{5\bullet})_2]$ starting from $H_2L^6\cdot HI$ and $H_2L^5\cdot HI$, respectively, and $Zn(OAc)_2\cdot 2H_2O$ led to the isolation of $(L^{6,ox})^0$ and the heterocyclic compound **11** (Scheme 4). The latter is an isomer of $(L^{5,ox})^0$, resulting from a (2+4) cycloaddition of one C−C double bond of the 4-phenyl ring with the N═C−N═N imine-hydrazone fragment, followed by rearomatization via a 1,3-H shift.

Figure 2 shows the electronic spectra of square planar complexes **1**−**3** and of their tetrahedral analogues **4**−**6**. The spectra of **1**−**3** are dominated by a very intense ($\epsilon \sim 1.5 \times 10^4$ M^{-1} cm^{-1}) spin and dipole allowed ligand-to-ligand charge-transfer band (LLCT) at 700−800 nm. This absorption maximum is typical for square planar nickel(II) complexes containing two π-radical monoanionic ligands.[19,20]

(15) Neese, F. *ORCA*, an ab Initio Density Functional and Semiempirical Electronic Structure Program Package, Version 2.3, Revision 07; Max-Planck-Institut für Bioanorganische Chemie: Mülheim, Germany, November 2003.
(16) (a) Becke, A. D. *J. Chem. Phys.* **1988**, *84*, 4524. (b) Perdew, J. P. *Phys. Rev.* **1986**, *33*, 8522. (c) Lee, C.; Yang, W.; Parr, R. G. *Phys. Rev. B.* **1988**, *37*, 785. (d) Becke, A. D. *J. Chem. Phys.* **1993**, *98*, 5648.
(17) (a) Schäfer, A.; Horn, H.; Ahlrichs, R. *J. Chem. Phys.* **1992**, *97*, 2571. (b) Schäfer, A.; Huber, C.; Ahlrichs, R. *J. Chem. Phys.* **1994**, *100*, 5829.
(18) (a) Neese, F. *Inorg. Chim. Acta* **2002**, *337*, 181. (b) Neese, F. *J. Chem. Phys.* **2003**, *119*, 9428.
(19) Herebian, D.; Bothe, E.; Neese, F.; Weyhermüller, T.; Wieghardt, K. *J. Am. Chem. Soc.* **2003**, *125*, 9116 and references therein.
(20) (a) Herebian, D.; Wieghardt, K.; Neese, F. *J. Am. Chem. Soc.* **2003**, *125*, 10997. (b) Ghosh, P.; Bill, E.; Weyhermüller, T.; Neese, F.; Wieghardt, K. *J. Am. Chem. Soc.* **2003**, *125*, 1293.

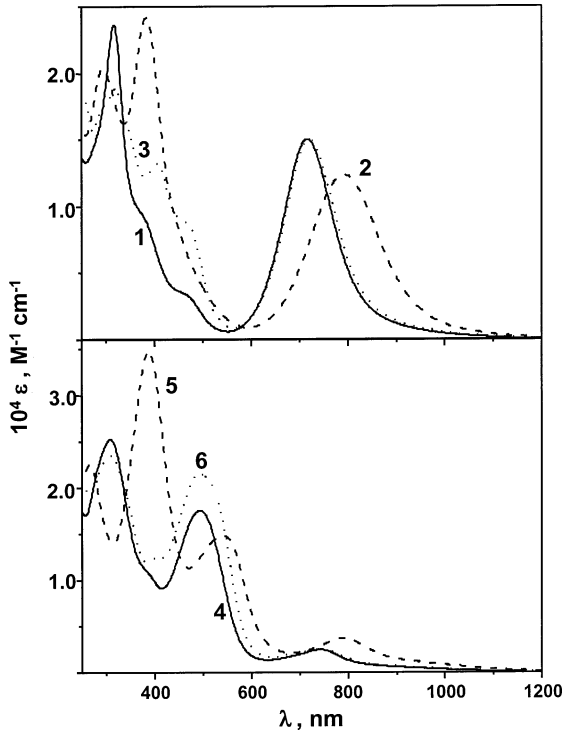

Figure 2. Electronic spectra of square planar complexes **1**, **2**, and **3** (top) and of tetrahedral species **4**, **5**, and **6** (bottom) in CH_2Cl_2 solution.

Significantly, this LLCT absorption is not observed in the spectra of tetrahedral complexes **4**−**6**.

The spectrum of octahedral **7** in CH_2Cl_2 displays a weak absorption maximum at 716 nm ($\epsilon \sim 1.8 \times 10^3\ M^{-1}\ cm^{-1}$), and stronger ones at 450sh (1.0×10^4), 380 (2.4×10^4). The latter bands are similar to those observed for the ligand **10**, ($L^{6,ox}$).

Crystal Structures. The crystal structures of **1** and **5**−**11** have been determined by X-ray crystallography; in all cases data sets have been collected at 100(2) K. The structures of **1** and **5** determined at 298 K have been described previously.[1,3] Agreement between these and the present structure determinations is excellent, but the average esd's of N−N, C−N, and C−C distances at 298 K is three to four times larger than those obtained from the 100 K data sets here. Thus, the accuracy of these redetermined structures of **1** and **5** has been significantly improved. Crystallographic data are summarized in Table 1; important bond distances are given in Table 2.

Figure 3 shows the structures of the neutral molecules [Ni^{II}-($L^{1\bullet}$)$_2$], [Ni^{II}($L^{5\bullet}$)$_2$], and [Ni^{II}($L^{6\bullet}$)$_2$] in crystals of **1**, **5**, and **6**, respectively. In all three cases, the C−N, N−N, and C−S bond distances of the five-membered chelate rings Ni−N_1−N_2−C_1−N_3 are identical within experimental error ($3\sigma \sim \pm 0.006$ Å): average N_1−N_2 at 1.342 Å, C_1−N_2 at 1.346 Å, C_1−N_3 at 1.324 Å, and C_1−S at 1.752 Å. This is a clear indication that the oxidation level of the ligand is the same in **1**, **5**, and **6** irrespective of the N-substituents or the geometry at the nickel(II) ion (square planar vs tetrahedral). In accordance with previous authors,[1−3] we conclude that the ligands are monoanionic π-radicals ($L^{1\bullet}$)$^{1-}$ in **1**, ($L^{5\bullet}$)$^{1-}$ in **5**, and ($L^{6\bullet}$)$^{1-}$ in **6**. This has also been shown for iron and cobalt complexes containing two π-radical anions derived from *S*-methyl-1-phenyl-isothiosemicarbazide.[5,6]

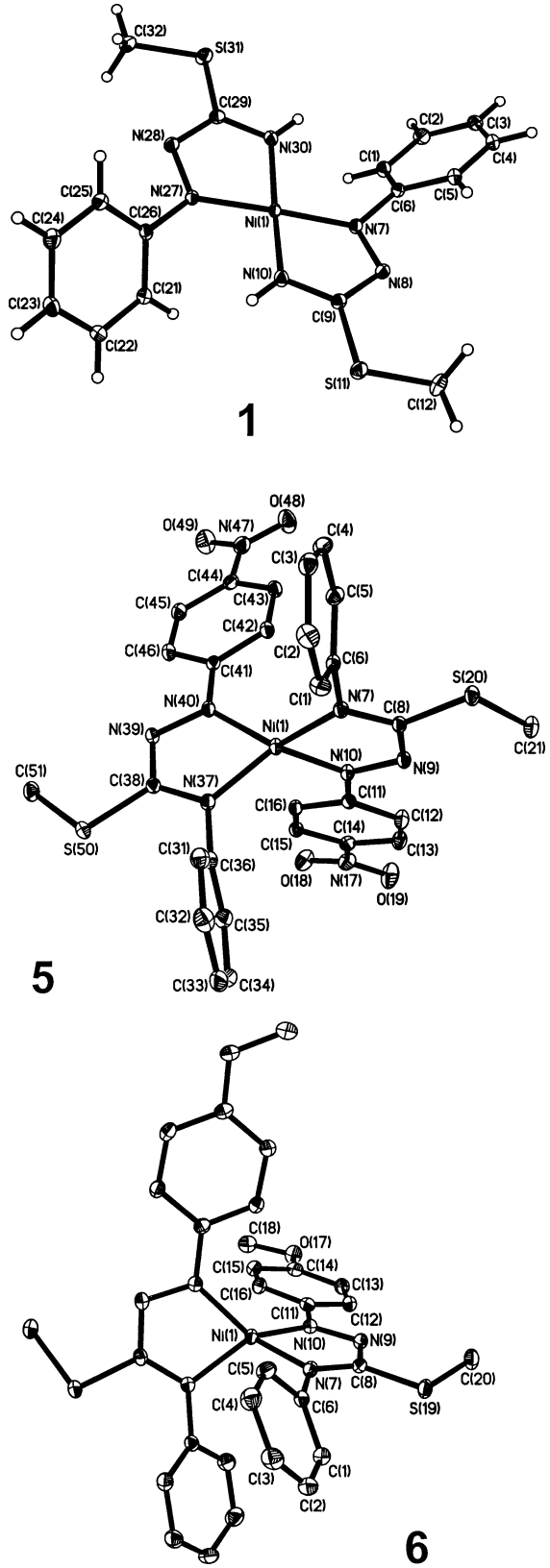

Figure 3. Structures of the neutral molecules in crystals of **1**, **5**, and **6**, respectively.

The two best planes defined each by the five atoms of the five-membered chelate rings in **1**, **5**, and **6** have dihedral angles of 12°, 85°, and 71°, respectively. Thus, the coordina-

Table 2. Selected Bond Distances (Å) and Angles (deg) of Complexes

complex 1			
Ni−N10	1.8387(9)	C6−N7	1.418(1)
Ni−N30	1.8434(9)	N7−N8	1.350(1)
Ni−N27	1.8518(8)	N8−C9	1.339(1)
Ni−N7	1.8524(8)	C9−N10	1.319(1)
C26−N27	1.417(1)	C9−S11	1.752(1)
N27−N28	1.350(1)	S11−C12	1.800(1)
N28−C29	1.339(1)	C29−S31	1.751(1)
C29−N30	1.322(1)	S31−C32	1.802(1)
N10−Ni−N27	98.41(4)	N10−Ni−N30	169.23(4)
N30−Ni−N27	81.51(4)	N27−Ni−N7	176.64(4)
N10−Ni−N7	81.51(4)		
N30−Ni−N7	99.20(4)		
complex 5			
Ni−N10	1.8905(9)	C6−N7	1.433(1)
Ni−N40	1.8970(9)	N7−C8	1.326(1)
Ni−N37	1.9070(9)	C8−N9	1.352(1)
Ni−N7	1.9200(9)	C8−S20	1.749(1)
N9−N10	1.333(1)	S20−C21	1.807(1)
N10−C11	1.407(1)	C36−N37	1.432(1)
C14−N17	1.465(1)	N37−C38	1.325(1)
C38−N39	1.355(1)	N40−C41	1.407(1)
C38−S50	1.750(1)		
N39−N40	1.336(1)		
N10−Ni−N40	122.19(4)	N40−Ni−N7	130.84(4)
N10−Ni−N37	124.92(4)	N37−Ni−N7	124.96(4)
N40−Ni−N37	80.20(4)		
N10−Ni−N7	80.39(4)		
complex 6			
Ni−N10	1.870(1)	N9−N10	1.343(2)
Ni−N7	1.913(1)	N10−C11	1.411(2)
C6−N7	1.418(2)	S19−C20	1.806(2)
N7−C8	1.328(2)		
C8−N9	1.346(2)		
C8−S19	1.758(2)		
N10−Ni−N10*	123.94(8)	N10*-Ni−N7*	80.68(6)
N7−Ni−N10*	134.90(6)	N10−Ni−N7*	134.90(6)
N10−Ni−N7	80.68(6)	N7−Ni−N7*	109.28(8)
complex 7			
Ni−I1	2.7523(2)	N8−C9	1.437(2)
Ni−N10	2.021(1)	C9−N10	1.276(2)
Ni−N7	2.113(1)	C9−S11	1.736(1)
C6−N7	1.427(2)	S11−C12	1.805(2)
N7−N8	1.267(2)		
N10*-Ni−N10	180.0		
N10*-Ni−N7	104.85(5)		
N10−Ni−N7	75.15(5)		
complex 8			
Ni−N30	2.019(5)	Ni−N7	2.144(5)
Ni−N50	2.030(4)	Ni−N27	2.168(5)
Ni−N10	2.031(5)	Ni−N47	2.180(4)
C6−N7	1.427(7)	C9−N10	1.277(7)
N7−N8	1.254(7)	C9−S11	1.722(6)
N8−C9	1.446(7)	S11−C12	1.798(6)
N27−N28	1.272(6)	N47−N48	1.265(6)
complex 9			
Ni−N10	2.068(2)	C6−N7	1.440(4)
Ni−N7	2.099(2)	N7−C8	1.290(4)
Ni−I31	2.7611(4)	C8−N9	1.440(4)
C8−S17	1.736(3)	N9−N10	1.259(3)
N10−C11	1.443(3)	S17−C18	1.811(3)
I31−I32	3.1193(5)	I32−I33	2.7808(4)
I33−I32−I31	174.65(1)	N10*-Ni−N7	104.86(9)
N10−Ni−N7	75.14(9)		
compound 10[a]			
C6−N7	1.421(6)	C8−S19	1.773(4)
N7−C8	1.262(5)	N9−N10	1.258(5)
C8−N9	1.435(5)	N10−C11	1.413(5)
S19−C20	1.799(5)		
compound 11[b]			
C1−C6	1.401(2)	C8−N9	1.289(2)
C6−N7	1.404(2)	C8−S20	1.753(2)
N7−C8	1.382(2)	S20−C21	1.803(2)
N9−N10	1.420(2)		
N10−C11	1.375(2)		

[a] Data for one coordinated ($L^{1,ox}$) are given. [b] Data for one of four crystallographically independent molecules are given.

tion geometry of the four nitrogen donors around the nickel(II) ions is best described as slightly distorted square planar in **1** and distorted tetrahedral in **5** and **6**. This dihedral angle is 0° in a completely planar bis(chelate)nickel complex and 90° in an ideal tetrahedron.

The two N,N-coordinated bidentate *S*-methyl-1-phenylisothiosemicarbazide ligands (irrespective of their oxidation level) can adopt a cis- or trans-configuration relative to each of the complexes with a square planar MN_4 polyhedron as shown in Scheme 5. Experimentally, only trans-configurated square planar species have been characterized to date as in **1** (and probably also **2** and **3**). It is now important to realize that in distorted tetrahedral complexes (**4**, **5**, and **6**) two geometrical isomers, namely, A and B in Scheme 5, exist if the dihedral angle, θ, between the two five-membered chelate rings is not 90° as in **5** and **6**. Both isomers A and B possess C_2 symmetry, but the intramolecular distance between the nitro groups in **5** (or the two methoxy groups in **6**) differ in both isomers if $\theta \neq 90°$. It is conceivable that A and B easily interconvert in solution.

The average Ni−N bond distances in square planar **1** are shorter at av. 1.85 Å than in the corresponding tetrahedral species **5** and **6** at 1.90 Å, which reflects the difference of ionic radii between a diamagnetic square planar Ni(II) ion (0.63 Å) and a paramagnetic tetrahedral one (0.69 Å).[21]

(21) Shannon, R. D. *Acta Crystallogr.* **1976**, *A32*, 751.

Scheme 5. Geometric Isomers

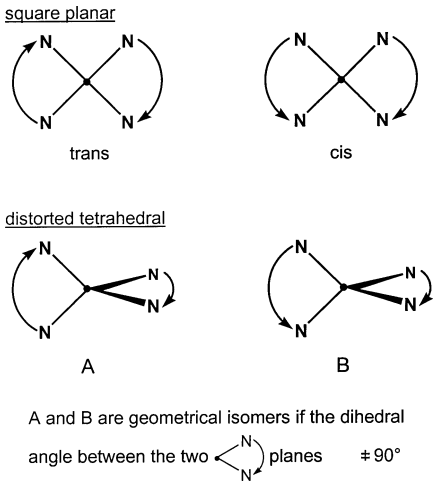

The crystal structure of octahedral *trans*-$[Ni^{II}(L^{1,ox})_2I_2]\cdot 2CHCl_3$, **7**·$2CHCl_3$, has been determined using a room-temperature data set.[2] Nonsolvated single crystals of **7** were grown by slow evaporation of a CH_2Cl_2/toluene mixture of **7**. Its crystal structure has been determined at 100(2) K. The new structure is significantly more accurate than the previous determination[2] but does not reveal structural differences of the neutral complex. Figure 4 exhibits the structures of **7** and **8**. The two five-membered chelate rings Ni−N_1−N_2−C_1−N_3 in **7** and three in the dication in crystals of **8** have

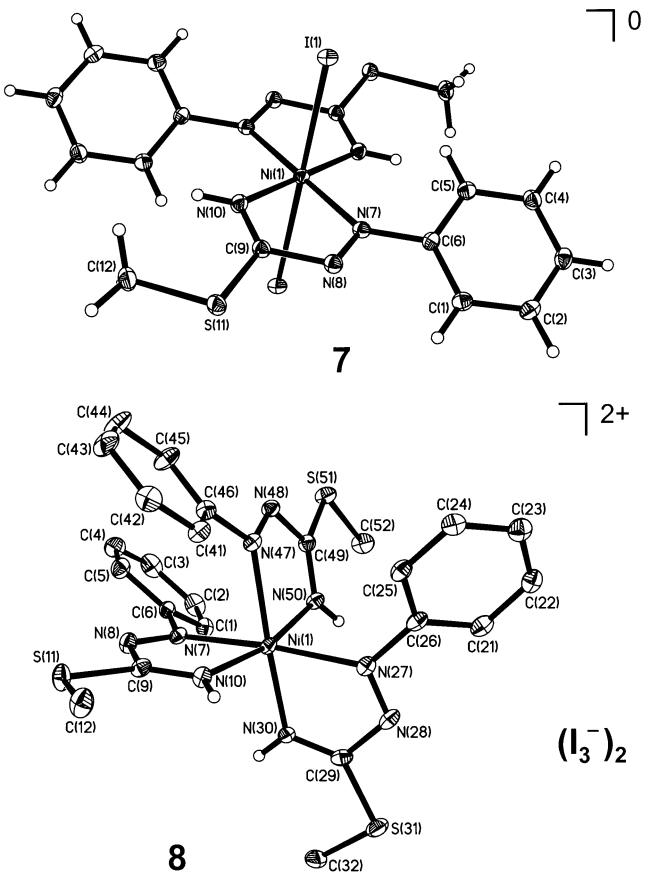

Figure 4. Structures of the neutral molecule in crystals of **7** (top) and of the dication in crystals of **8** (bottom).

identical N−N, C−N, C−S bond distances, which clearly differ from those in **1**, **5**, and **6**. Remarkably, the average N_1-N_2 bond length at 1.265 Å is significantly shorter than in **1**, **5**, and **6**; it indicates the presence of an N═N double bond. Similarly, the average C_1-N_3 bond length at 1.277 Å indicates the presence of a C═N double bond, whereas the C_1-N_2 bond at 1.438 Å is representative of a C−N single bond. Thus, the ligands in **7** and **8** are the diamagnetic, neutral form as in **10**.

Figure 5 shows the structure of the neutral molecule *trans*-$[Ni^{II}(L^{5,ox})_2(I_3)_2]$ in crystals of **9**. The two 1,4-diphenyl ligand derivatives ($L^{5,ox}$) are coordinated in trans-position relative to each other, the NiN_4 moiety being completely planar. The two neutral ligands $(L^{5,ox})^0$ are each N,N-bound in a fashion that maximizes the intramolecular distance between the two nitro substituents (they are in trans-position with respect to each other). The phenyl group of one ($L^{5,ox}$) ligand and the nitrophenyl group of the other are opposite to each other in the neutral molecule; the dihedral angle between these two phenyl rings is 7.8° and the distance between the centroids of both rings is 3.465 Å indicative of a weak π-stacking. Thus, there appears to be no steric hindrance between the two ligands when coordinated in a "planar" manner in **9**. The average Ni−N distance in octahedral at 2.083 Å is longer than in square planar **1** at 1.847 Å. Simple geometrical considerations then yield a ring-to-ring π-stacking distance of 2.8−2.9 Å in a hypothetical square planar $[Ni(L^{5\bullet})_2]$ complex. This π-stacking distance may be too short and may

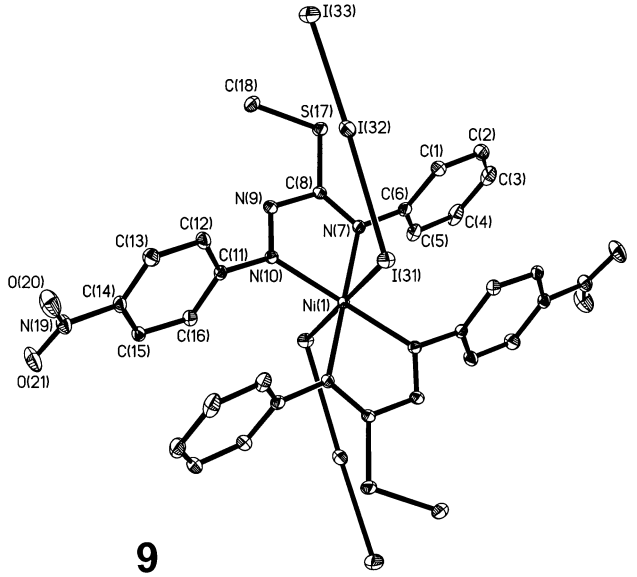

Figure 5. Structure of neutral molecule *trans*-$[Ni^{II}(L^{5,ox})_2(I_3)_2]$ in crystals of **9**.

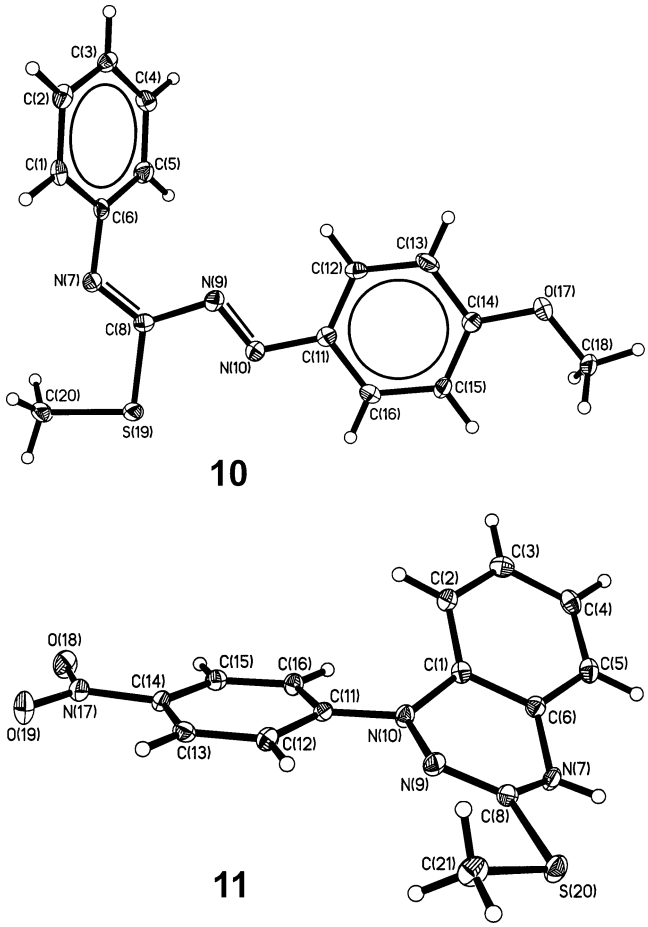

Figure 6. Structures of neutral molecules in crystals of **10** (top) and **11** (bottom).

explain why $[Ni(L^{5\bullet})_2]$ (**5**) favors a tetrahedral structure, but the situation is borderline. In $\{[Pd(bpy)(B^{\bullet})](PF_6)\}_2$ the ring-to-ring distance of the π-radical of *o*-phenylenediamine, $(B^{\bullet})^{1-}$, is only 2.92 Å.[22]

Figure 6 displays the crystal structures of neutral **10** and **11**, both of which do not contain a transition metal ion. **10**

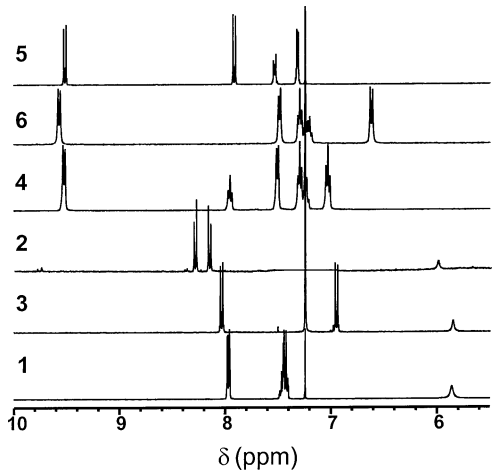

Figure 7. 400 MHz ^{1}H NMR spectra of complexes **1**−**6** ($CDCl_3$) at 300 K in the range 5.8−10 ppm.

Table 3. 400 MHz ^{1}H NMR Spectra of Free Ligands and Complexes

species[a]	δ(*o*-HArNN proton)[b]	δ(*m*-HArNN proton)[c]
H_2 L^1·HI	6.79	7.27
H_2 L^2·HI	6.92	8.17
H_2 L^3·HI	6.76	6.86
1	7.97	7.43
2	8.16	8.29
3	8.03	6.95
4	9.52	7.03
5	9.52	7.91
6	9.57	6.61

[a] Spectra of free ligands were measured in CD_3OD and those of complexes **1**−**6** in $CDCl_3$ at 300 K. [b] Chemical shift values are given in ppm for the ortho hydrogens of the 1-phenyl group of the ligand. [c] Chemical shift values are given in ppm for the meta hydrogens of the 1-phenyl group of the ligand.

represents $(L^{6,ox})^0$, whereas **11** is a cyclic isomer of $(L^{5,ox})^0$. The short N−N bond at 1.262(2) Å in **10** represents a double bond, whereas the same bond in **11** at 1.420(5) Å is typical for a single bond in agreement with the formula shown in Scheme 4.

NMR Studies of 1−6. Since all $[Ni(L^{x\bullet})_2]$ complexes (**1**−**6**) possess a diamagnetic ground-state irrespective of the presence of a tetrahedral coordination polyhedron as in **4**−**6** or a square planar one as in **1**−**3**, the NMR spectra have been investigated to explore the possibility of an equilibrium between the two forms in solution. The 1-D and 2-D NMR spectra of **1** and **4**−**6** were recorded and analyzed. Complexes **2** and **3** are quite insoluble, and, therefore, only their ^{1}H NMR spectra were recorded.

Figure 7 shows the ^{1}H NMR spectra of **1**−**6** in the region 5.8 to 10 ppm at 300 K. In all cases only a single set of signals for the two coordinated ligands is observed indicating that both ligands are magnetically equivalent on the NMR time scale. A single broad N−H signal is observed for the square planar complexes at 5.88 ppm for **1**, 5.99 ppm for **2**, and 5.85 ppm for **3**; **4**−**6** do not display such a signal. Table 3 summarizes the values of the chemical shift, δ, of the 1-phenyl protons in the ortho (*o*-HArNN) and meta (*m*-HArNN) positions opposite the hydrazine substituent for the three uncoordinated $H_2[L^{1-3}]$·HI ligands and the six complexes **1**−**6**. We note that the chemical shift values of the meta-protons in the uncoordinated ligand and the corresponding nickel complex are similar and only slightly shifted upon complexation to lower fields by 0.16 ppm (R = H), 0.12 (R = NO_2), and 0.09 ppm (R = OCH_3). In contrast, in the same series the signals of the ortho protons increase by 1.18 ppm (R = H), 1.24 ppm (R = NO_2), and 1.17 ppm (R = OCH_3). Such a variation cannot originate from simple solvent effects; it confirms, instead, the presence of coordinated species in solution. Moreover, this rather drastic change indicates an important electronic modification in the nature of ortho-C−H bonds. We attribute this change to the ligand oxidation on going from the uncoordinated, closed-shell ligands to the coordinated radicals in $[Ni(L^{R\bullet})_2]$.

Interestingly, the *o*-HArNN proton signals of the three tetrahedral $[Ni(L^{R\bullet}{}_{Ph})_2]$ complexes are much more deshielded with 9.52 ppm for **4**, and **5**, and 9.57 ppm for **6** than those of the square planar complexes $[Ni(L^{R\bullet})_2]$ with 7.43 for **1**, 8.29 ppm for **2**, and 6.95 ppm for **3**. Thus, the tetrahedral and square planar complexes exhibit significantly different signals in solution at ambient temperature. No additional peaks or coalescence processes were observed in the spectrum of $[Ni(L^{1\bullet})_2]$ (**1**) recorded in CD_2Cl_2 in the temperature range 300 to 215 K. Thus, the tetrahedral and square planar complexes are not in equilibrium; they remain intact in their given coordination polyhedron even in solution.

Table 4. Redox Potentials of Complexes[a]

complex	E^p_{ox}, V^b	E^p_{red}, V^c	$E^1_{1/2}$ (0/−1), V^d	$E^2_{1/2}$ (−1/−2) V^d	K_d[e]
1[19]	0.05	−0.24	−1.24	−1.865	2.6×10^{-5}
2	0.22	0.0	−0.75	−0.97	2.4×10^{-2}
3	−0.03	0.15, 0.26	−1.29	−2.01	1.0×10^{-6}
4	0.07	0.10	−1.31	−1.64	3.6×10^{-3}
5[f]	0.37	0.15	−0.85	−1.01	6.6×10^{-2}
6	0.04	−0.15	−1.43	−1.80	2.1×10^{-3}

[a] Referenced vs the F_c^+/F_c couple. [b] Peak potential for oxidation. [c] peak potential for the corresponding reduction(s). [d] Half-wave potentials for the 0/−1 (and −1/−2) couple. [e] Disproportionation constant according to eqs 1 and 2. [f] $E^3_{1/2}$ (−2/−3) is observed at −2.02 V. Conditions: scan rate 100 mV s^{-1}; 20 °C; CH_2Cl_2 solution (0.20 M $[(n\text{-}Bu)_4N]PF_6$).

Electro- and Spectroelectrochemistry. The electrochemistry of complexes **1**−**6** has been studied in CH_2Cl_2 solutions containing 0.2 M $[(n\text{-}Bu)_4N]PF_6$ as supporting electrolyte by cyclic voltammetry (cv). Ferrocene was used as internal standard; all redox potentials are referenced versus the ferrocenium/ferrocene (Fc^+/Fc) couple, and the results are summarized in Table 4. In general, the complex concentration was in the millimolar range, but low solubility of **2** and **3** enforced lower concentrations at ∼0.1 mM for **3** and ∼10 μM for **2**. The cv of **1** has been reported previously.[23]

As shown in Figure 8, the complexes display very similar electrochemical behavior irrespective of the coordination polyhedron (square planar **1**−**3** or tetrahedral **4**−**6**): all undergo a two-electron oxidation in the range −0.03 to 0.40

(22) Ghosh, P.; Begum, A.; Herebian, D.; Bothe, E.; Hildenbrand, K.; Weyhermüller, T.; Wieghardt, K. *Angew. Chem., Int. Ed.* **2003**, *42*, 563.

(23) The cyclic voltammogram of **1** in acetonitrile has been reported: Tarazewska, J.; Revenco, M. D.; Timco, L. *Pol. J. Chem.* **1997**, *71*, 253.

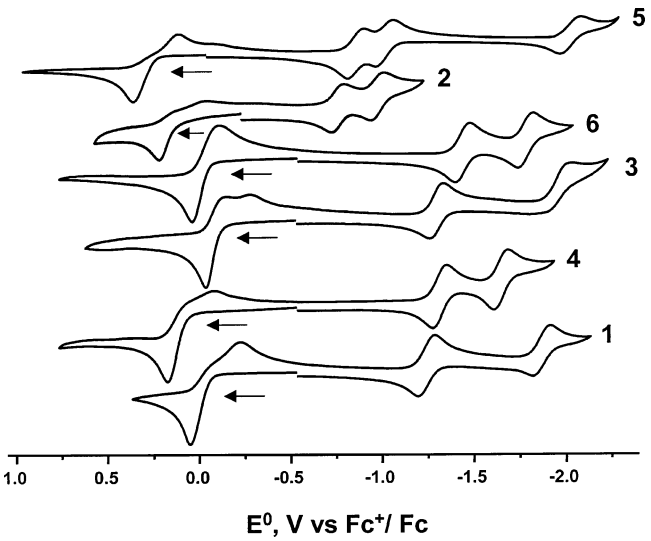

Figure 8. Cyclic voltammograms of complexes **1**−**6** in CH_2Cl_2 solution [0.20 M $[N(n\text{-}Bu)_4]PF_6$ supporting electrolyte, glassy carbon working electrode, 20 °C, ferrocene (Fc) internal standard, scan rate 100 mV s^{-1}].

V and a two-electron reduction in the range −0.2 to 0.0 V. These waves have irreversible character ($\Delta E_p \sim 300$ mV) and have not been investigated further. In addition, all complexes display two successive, reversible one-electron reduction waves. Only complex **5** exhibits an additional reversible one-electron reduction at $E^3_{1/2} = -2.02$ V, which we assign to a metal-centered reduction Ni^{II}/Ni^{I} of the couple $[Ni^{II}(L^5)_2]^{2-}/[Ni^{I}(L^5)_2]^{3-}$.

The redox potentials within the series of square planar complexes **1**−**3** clearly vary as a function of the nature of the p-substituent of the 1-phenyl group: the electron-withdrawing properties of the nitro group in **2** makes the neutral species more difficult to oxidize (by ∼0.2 V) and easier to reduce (by 0.4 or 0.9 V) than the corresponding unsubstituted species **1**.

For the methoxy electron-donating substituted species **3** the opposite trends are observed in comparison with the data for unsubstituted **1**. Similar trends hold for the tetrahedral complexes **4**−**6**.

The disproportionation constant (corresponding to a comproportionation constant $K_c = K_d^{-1}$) for the equilibrium between the monoanionic forms of complexes **1**−**6** and their neutral and dianionic forms eq 1 can be calculated by use of eq 2.

$$2\,[Ni^{II}(L^{x\bullet})(L^{x,red})]^- \overset{K_d}{\rightleftharpoons} [Ni^{II}(L^{x,red})_2]^{2-} + [Ni(L^{x\bullet})_2]^0 \quad (1)$$

$$K_d = \exp\,(nF(E^2_{1/2} - E^1_{1/2})/RT = \exp((E^2_{1/2} - E^1_{1/2})/0.059) \quad (2)$$

The results are summarized in Table 4. A small value of K_d (or a large one for K_c) as for square planar **1** and **3** indicates a relatively large electronic stabilization of the corresponding square planar mixed valent monoanion, i.e., this species is probably a class III mixed valent species where the unpaired electron is delocalized over both ligands. It is unclear to us why K_d of **2** is so large since the electronic spectrum of its monoanion is very similar to that of $[\mathbf{1}]^-$ and $[\mathbf{3}]^-$, indicating a ligand mixed valency of class III. In contrast, K_d for the tetrahedral species **4**, **5**, and **6** is larger by at least 3 orders of magnitude. We take this as an indication that the corresponding mixed valent monoanions possess a more localized electronic structure $[Ni^{II}(L^{x,red})(L^{x\bullet})]^-$ (class I or II).

Table 5. Electronic Spectra in CH_2Cl_2 Solution

complex[a]	λ_{max}, nm ($10^4\,\epsilon$, $M^{-1}\,cm^{-1}$)
1	710(1.5), 465sh(0.5), 370sh(1.0), 310(2.6)
$[\mathbf{1}]^-$	1120(101), 390(1.1), 305(2.5)
$[\mathbf{1}]^{2-}$	405(1.8), 295(2.4)
2	795(1.2), 385(2.5), 290(1.7)
$[\mathbf{2}]^-$	1385(1.2), 755(1.2), 480(2.6)
$[\mathbf{2}]^{2-}$	760(3.1), 555(2.0), 475(2.2), 365(1.0), 255(1.9)
3	720(1.5), 465sh(0.8), 405(1.2), 315(1.7), 296sh(1.6)
$[\mathbf{3}]^-$	1115(1.0), 390(1.1), 305(2.1)
4	900(0.1), 745(0.3), 495(1.7), 381sh(1.1), 305(2.5), 240(1.8)
$[\mathbf{4}]^-$	905(0.1), 745(0.3), 490(1.1), 300(2.2), 240(2.0)
$[\mathbf{4}]^{2-}$	910(0.2), 700sh(0.3), 600sh(0.4), 475(0.6), 345sh(2.3), 320(2.3), 243(2.2)
5	800(0.5), 545(1.5), 390(3.7), 265(2.4)
$[\mathbf{5}]^-$	665(1.6), 495(2.7), 410(2.3)
$[\mathbf{5}]^{2-}$	710(4.1), 650(3.9), 595(5.1), 555sh(3.7), 470sh(2.0), 360(1.6), 305(1.9)
6	750(0.3), 495(2.1), 405(1.3), 310(2.3), 265(2.0)
$[\mathbf{6}]^-$	905(0.2), 705(0.3), 480(1.0), 315(2.6), 255(2.2)
$[\mathbf{6}]^{2-}$	650sh(0.3), 485sh(0.7), 360(2.9), 330(2.8), 250(2.2)
7	715(0.2), 435sh(0.9), 340(2.5)
[**9**]	790(0.5), 535(2.2), 385(4.8), 265(3.4)
[**10**]	495(0.2), 358(2.1)

[a] The mono- and dianions were generated electrochemically in CH_2Cl_2 solutions (0.20 M $[N(n\text{-}Bu)_4]PF_6$).

Controlled potential electrolysis at −20 °C of CH_2Cl_2 solutions of the neutral complexes **1**−**6** (0.20 M $[(n\text{-}Bu)_4N]PF_6$) at appropriately fixed negative potentials allowed the generation of stable solutions containing the corresponding mono- or dianions, for which it has been possible to record their electronic spectra (Table 5). An example for **1**, $[\mathbf{1}]^-$, and $[\mathbf{1}]^{2-}$ is shown in Figure 9. It is remarkable that the ligand-to-ligand charge-transfer band (LLCT) at 717 nm ($\epsilon = 1.5 \times 10^4\ M^{-1}\ cm^{-1}$) of **1** is shifted to 1122 nm ($\epsilon = 1.06 \times 10^4\ M^{-1}\ cm^{-1}$) upon one-electron reduction to the monoanion and disappears completely upon further one-electron reduction yielding the dianion. This is excellent evidence that both reductions are ligand-centered processes, eq 3.[19,20]

$$[Ni^{II}(L^{1\bullet})_2] \overset{-e}{\underset{+e}{\rightleftharpoons}} [Ni^{II}(L^1)(L^{1\bullet})]^- \overset{-e}{\underset{+e}{\rightleftharpoons}} [Ni^{II}(L^1)_2]^{2-} \quad (3)$$

Similarly, the LLCT band at 722 nm ($\epsilon = 1.5 \times 10^4\ M^{-1}\ cm^{-1}$) for **3** shifts to 1115 nm ($\epsilon = 1.0 \times 10^4\ M^{-1}\ cm^{-1}$) in the monoanion (Figure S3, Supporting Information). For the nitro complex **2** (Figure 9), the shift of the LLCT band is observed from 795 nm ($\epsilon = 1.1 \times 10^4\ M^{-1}\ cm^{-1}$) to 1385 nm ($\epsilon = 1.25 \times 10^4\ M^{-1}\ cm^{-1}$). The spectrum of $[\mathbf{2}]^-$ also displays an intense band at 756 nm ($\epsilon = 1.15 \times 10^4\ M^{-1}\ cm^{-1}$), which increases in intensity to $\epsilon = 3.45 \times 10^4\ M^{-1}\ cm^{-1}$ upon generating the dianion $[\mathbf{2}]^{2-}$ while the LLCT band at 1400 nm disappears. We propose that the 756 nm band corresponds to a $\pi-\pi^*$ transition of the dianionic form of the nitro ligand $H_2[L^3]$. In the N,N-coordinated dianion the strong electron acceptor nitro substituent is in the para

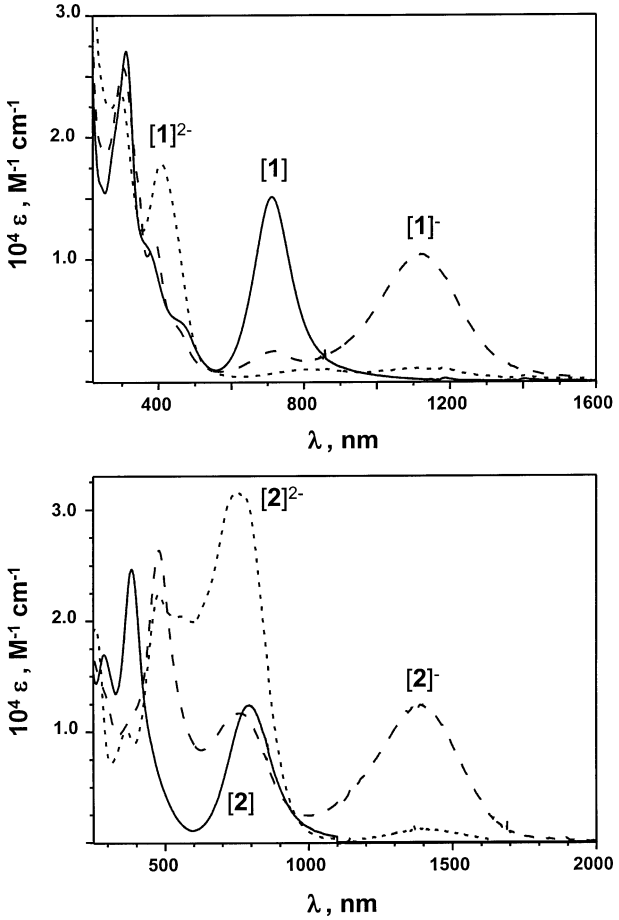

Figure 9. Electronic spectra of electrochemically generated mono- and dianions of **1** (top) and **2** (bottom) in CH_2Cl_2 solutions (0.2 M $[N(n\text{-}Bu)_4]PF_6$).

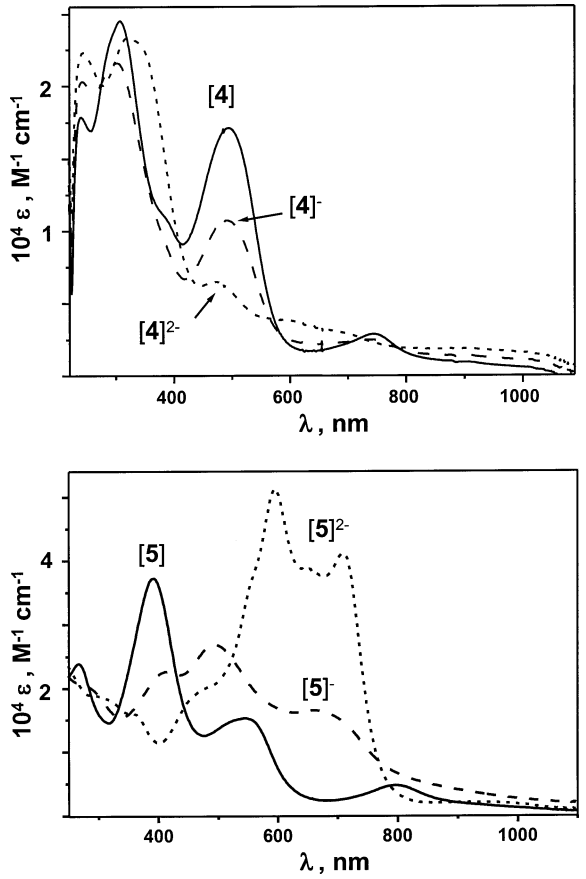

Figure 10. Electronic spectra of electrochemically generated mono- and dianions of **4** (top) and **5** (bottom) in CH_2Cl_2 solutions (0.20 M $[N(n\text{-}Bu)_4]PF_6$).

position of an aromatic phenyl ring with a strong electron donating hydrazido function: the molecule displays the characteristic behavior of an organic dye. These results clearly indicate that the monoanions of **1**−**3** are also square planar species.

The tetrahedral complexes **4**−**6** display this LLCT band neither in the neutral nor in their monoanionic forms, suggesting that these complexes remain tetrahedral upon reduction. The spectral changes observed are shown in Figure 10 for **4** upon reduction to $[\mathbf{4}]^-$ and $[\mathbf{4}]^{2-}$. It is noted that these reductions proceed with retention of isosbestic points, which indicates the clean formation of the mono- and dianionic forms from neutral **4**−**6**.

Figure 10 displays the electronic spectra of the nitro complexes **5**, $[\mathbf{5}]^-$, and $[\mathbf{5}]^{2-}$. In contrast to the results for **4** and **6** (Figure S4, Supporting Information), the evolution of spectra upon one- and two-electron reduction is dominated by an increase of absorption in the visible region. As has been discussed for the spectral changes of **2** upon reduction, this increase in absorption can be understood as a result of $\pi-\pi^*$ transition within the N,N-coordinated ligand dianion $[L^5]^{2-}$ (nitro-hydrazide push−pull mechanism). This would, at the same time, indicate that both reductions of tetrahedral **4**−**6** are ligand-centered processes. The lack of such LLCT bands for the monoanions indicates that they are also tetrahedral containing localized, N,N-coordinated mono- and dianionic ligands and central Ni(II) ions, $[Ni^{II}(L^{x\bullet})(L^x)]^-$ ($x = 4-6$).

Electron Spin Resonance Spectra of the Monoanions $[Ni^{II}(L^{x\bullet})(L^x)]^-$ (x = 1−6). The monoanionic forms of complexes **1**−**6**, namely, square planar or tetrahedral $[Ni^{II}(L^{x\bullet})(L^x)]^-$ species, have been generated electrochemically from the neutral forms **1** − **6** in CH_2Cl_2 solutions containing 0.2 M $[(n\text{-}Bu)_4N]PF_6$. All of them possess an $S = {}^1/_2$ ground state and display characteristic X-band EPR spectra as shown in Table 6.

The EPR spectra of the monoanionic forms of complexes **1**−**3** exhibit quasi- rhombic signals that are very similar to those reported for monoanionic species of $[NiL_2]$ where L represents a dioxolene type ligand.[24−26] Figure 11 shows the spectrum of $[\mathbf{1}]^-$; those for $[\mathbf{2}]^-$ and $[\mathbf{3}]^-$ are shown in Figure S5 (Supporting Information). The relative large g-anisotropy of these square planar monoanions has been traced[25,26] to the nature of the SOMO involved. This SOMO has been shown to be ligand-centered but with symmetry allowed, significant mixing of a d metal orbital yielding a ground state with sizable orbital angular momentum. This mechanism

(24) Chaudhuri, P.; Verani, C. N.; Bill, E.; Bothe, E.; Weyhermüller, T.; Wieghardt, K. *J. Am. Chem. Soc.* **2001**, *123*, 2213.
(25) Herebian, D.; Bothe, E.; Bill, E.; Weyhermüller, T.; Wieghardt, K. *J. Am. Chem. Soc.* **2001**, *123*, 10012.
(26) Sun, X.; Chun, H.; Hildenbrand, K.; Bothe, E.; Weyhermüller, T.; Neese, F.; Wieghardt, K. *Inorg. Chem.* **2002**, *41*, 4296.

Table 6. X-band EPR Spectra of Electrochemically Generated Monoanions of Complexes **1**−**6** in CH_2Cl_2 Solution (0.2 M $[(n\text{-Bu})_4N]PF_6$) at −20 °C

complex	g_x	g_y	g_z	g_{iso}	liquid N_{2+} freezing process (%)	pentane/ liquid N_2 process (%)
$[\mathbf{1}]^-$	2.081	2.011	2.004	2.032		
$[\mathbf{2}]^-$	2.067	2.027	2.008	2.034		
$[\mathbf{3}]^-$	2.080	2.018	2.009	2.063		
square planar $[Ni(L_{calcd})_2]^-$ [a]	2.077	2.014	1.994	2.028		
$[\mathbf{4}]^-$ subspecies a	2.265	2.157	2.008	2.143	72	58
subspecies b	2.215	2.133	2.043	2.130	28	42
$[\mathbf{5}]^-$ subspecies a	2.31	2.17	2.01	2.163	65	
subspecies b	2.22	2.12	2.03	2.12	35	
$[\mathbf{6}]^-$ subspecies a	2.257	2.160	2.011	2.143	85	63
subspecies b	2.198	2.137	2.043	2.126	15	37
$[\mathbf{6}]^-$ [a]	2.205	2.198	2.037	2.147		

[a] From DFT calculations (see text).

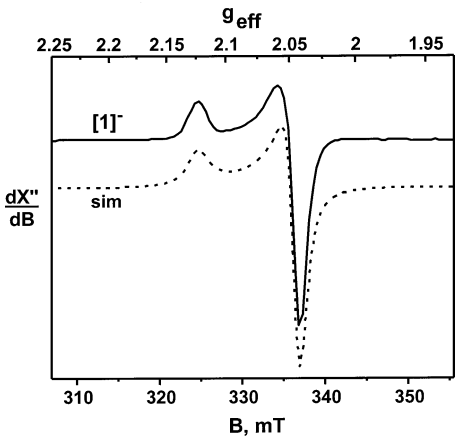

Figure 11. X-band EPR spectrum of electrochemically generated $[\mathbf{1}]^-$ in CH_2Cl_2 solution (0.2 M $[N(n\text{-Bu})_4]PF_6$) at 10 K.

requires a square planar configuration of the monoanions of **1**−**3**. No resolved hyperfine coupling to the nitrogen donor atoms has been observed. The *g* values are given in Table 6.

Figure 12 exhibits the X-band EPR spectrum of a frozen CH_2Cl_2 solution of electrochemically generated $[\mathbf{4}]^-$ at 80 K. To our surprise, this spectrum could only be satisfactorily simulated by taking into account *two* subspectra **a** and **b**. Both spectra display rather similar but not identical g_x, g_y, g_z values (Table 6). The ratio of species **a**/**b** was found to be 58:42 when the −20 °C electrochemically generated solution of $[\mathbf{4}]^-$ was shock-frozen in a liquid *n*-pentane/liquid dinitrogen bath. Upon changing the freezing procedure by using pure liquid dinitrogen, the resulting frozen solution contains the two species **a** and **b** in a ratio 72:28. These experiments clearly show that species **a** and **b** are in a thermodynamic equilibrium in solution with rapid transformation rates. From biological studies it is well-known that the heat transfer rates in liquid N_2 differ markedly from those in liquid *n*-pentane/N_2 (it is slow in the former and faster in the latter process).

It is quite remarkable that $[\mathbf{5}]^-$ and $[\mathbf{6}]^-$ display the same behavior. In each case two isomers, namely, **a** and **b**, exist

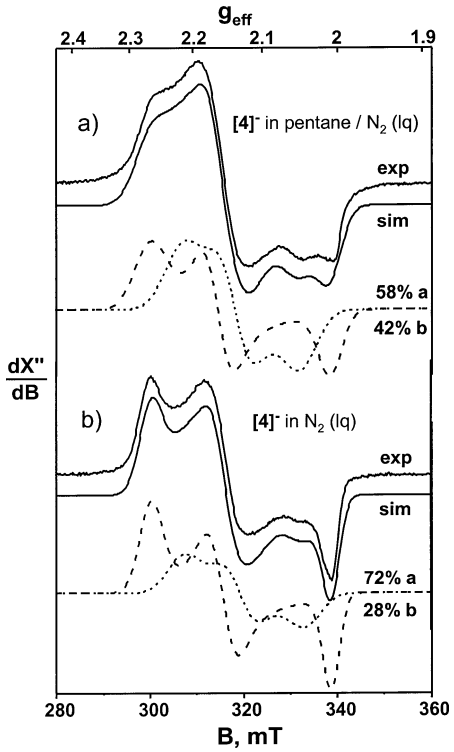

Figure 12. X-band EPR spectrum of electrochemically generated $[\mathbf{4}]^-$ in CH_2Cl_2 solution (0.2 M $[N(n\text{-Bu})_4]PF_6$) at 80 K. (a) Spectrum of shock frozen sample in a liquid *n*-heptane/N_2 mixture and (b) in liquid N_2. Two subspectra **a** with $g_x = 2.265$, $g_y = 2.157$, $g_z = 2.008$ and **b** with $g_x = 2.215$, $g_y = 2.133$, $g_z = 2.043$.

in an equilibrium. The EPR spectra are shown in Figures S6 and S7 (Supporting Information), respectively.

We note that the g-anisotropy of the monoanions $[\mathbf{4}]^-$, $[\mathbf{5}]^-$, and $[\mathbf{6}]^-$ (irrespective of their configuration **a** or **b**) is significantly larger than is observed for the square planar monoanions $[\mathbf{1}]^-$, $[\mathbf{2}]^-$, or $[\mathbf{3}]^-$. This rules out the possibility that the monoanions $[\mathbf{4}]^-$, $[\mathbf{5}]^-$ and $[\mathbf{6}]^-$ exist in a square planar configuration in solution. It would appear that both configurations **a** and **b** are in a distorted *tetrahedral* environment.

The solid-state structures of **5** and **6** have revealed an interesting facet. In both structures, the NiN_4 polyhedron is that of a severely distorted tetrahedron. The two ligand planes defined each by the five-membered chelate $\overline{Ni-N_1-N_2-C_1-N_3}$ form in **5** and **6** a dihedral angle of 84° and 65° (and not 90° as is required for an ideal tetrahedron). Thus, in a distorted tetrahedral complex containing two identical but asymmetric bidentate ligands the two geometrical configurations A and B shown in Scheme 5 exist. We propose that these two isomers are in equilibrium in the $[\mathbf{4}]^-$, $[\mathbf{5}]^-$, and $[\mathbf{6}]^-$; they can easily and rapidly be interconverted.

Calculations. In this section, a detailed picture of the electronic structures of the neutral $[Ni^{II}(L^{x\bullet})_2]$ complexes and of their corresponding monoanions will be developed. In an attempt to dissect influences of electronic from steric effects, we calculated a truncated (small) model that is labeled $[Ni(L^{\bullet}_{calcd})_2]$ where $(L^{\bullet}_{calcd})^{1-}$ is $(HN-N{=}C(SH)NH^{\bullet})^{1-}$. The coordination geometry of the complex was assumed to be tetrahedral and/or square planar. Then we calculated the

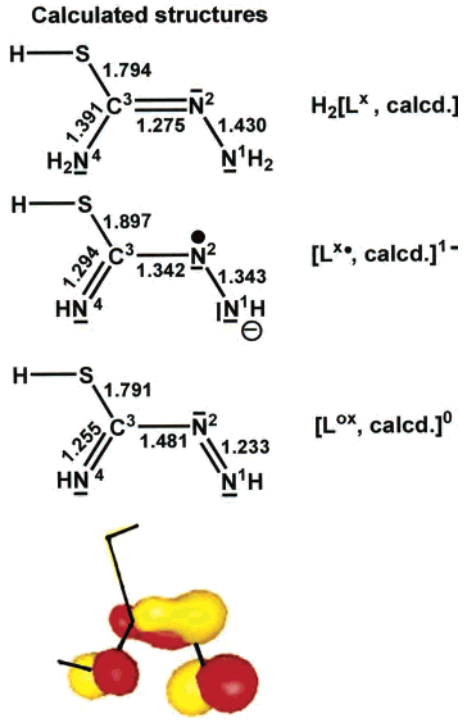

Figure 13. Calculated bond distances in the free ligands $H_2[L_{calcd}]$, $[L^{\bullet}_{calcd}]^{1-}$, and $[L^{ox}_{calcd}]^0$. The HOMO of $H_2[L_{calcd}]$ is also shown (it is the SOMO in $[L^{\bullet}_{calcd}]^{1-}$ and the LUMO in $[L^{ox}_{calcd}]^0$).

structures of **1**, **5**, and **6** and the corresponding monoanionic forms thereof.

It is educational to calculate the structure of the ligand in three different oxidation levels first: the optimized geometries of ($H_2N-N=C(SH)NH_2$) (H_2L_{calcd}); its anionic radical ($HN-N=C(SH)NH^{\bullet}$)$^{1-}$, ($L^{\bullet}_{calcd}$)$^{1-}$, and of the neutral oxidized molecule HN=N−C(SH)=NH, (L^{ox}_{calcd}), were elucidated. The results of the B3LYP optimizations are shown in Figure 13 together with the redox-active orbital, which is the LUMO of (L^{ox}_{calcd}), the SOMO for ($L^{\bullet}_{calcd}$)$^{1-}$, and the HOMO for H_2L_{calcd}. This orbital is antibonding between the two hydrazine nitrogens, N1−N2, but bonding between N_2-C_3 and antibonding between C_3-N_4. Thus, upon reduction from L^{ox} to $H_2[L_{calcd}]$ the N_1-N_2 and C_3-N_4 bond lengths increase while that of N_2-C_3 decreases. Gratifyingly, these calculated bond distances for the radical anion agree nicely with those determined experimentally in **1**, **5**, and **6** and for L^{ox}_{calcd} with those in **7**, **8**, **9**, and **10**.

1. Calculated Geometries of Square Planar Complexes. Consistent with the notion that the square planar complexes $[Ni^{II}(L^{\bullet}_{calc})_2]$ and $[Ni^{II}(L^{1\bullet})_2]$ (**1**) contain two radical ligands, the ground-state geometries for these two neutral molecules were optimized in the high-spin state (S = 1) and in the corresponding broken symmetry (BS) diamagnetic $M_s = 0$ state.

Using the BP86 functional, we found that the BS state does not exist; all calculations converged to a closed shell state. In contrast, using the B3LYP functional, the BS solutions exist and they are lower in energy than the corresponding high-spin states. Such discrepancy between the two functionals has previously been noticed.[20] However, although describing different electronic structures, the bond lengths in both calculated geometries of $[Ni^{II}(L^{1\bullet})_2]$ are very similar and very close to those of the experimental structure (Table 2). In particular, the N1−N2, N2−C3, and C3−N4 bond lengths are in both cases in excellent agreement with the experimental findings and characteristic of a radical monoanion form of the ligand. Finally, the B3LYP calculations, with $d_{Ni-N} = 1.891$ Å, gave a slightly longer average Ni−N bond distance than BP86 calculations ($d_{Ni-N} = 1.862$ Å). They are both longer than the experimental value at 1.847 Å. Both functionals tend also to overestimate the dihedral angle between the two NCNNNi metallacycles, with angles of 19° and 22°, respectively, as compared to an experimental value of 12°.

The B3LYP calculated geometry of the truncated model, $[Ni^{II}(L^{\bullet}_{calc})_2]$, displays the main characteristics of the experimental findings. However, the two NCNNNi metallacycles are coplanar, suggesting that the twist found in the experimental structure is related to steric interactions involving the 1-phenyl rings. This decrease of the dihedral angle in the truncated model is associated with a decrease of the Ni−N average bond distance from 1.891 Å in $[Ni^{II}(L^{1\bullet})_2]$ (**1**) to 1.861 Å in $[Ni^{II}(L^{\bullet}_{calc})_2]$. It has been shown previously for related complexes[20] that the metal character of the $3b_g$ MO (see electronic structure below) indicates that there is significant metal-to-ligand π-back-donation. The difference in Ni−N bond length is therefore likely to be related to a larger π-back-bonding interaction from the nickel to the ligand in a true square planar environment as compared to a distorted one.

For the square planar monoanions, $[Ni^{II}(L^1)_2]^-$ and $[Ni^{II}(L_{calc})_2]^-$, the geometries were optimized in spin-unrestricted $S = {}^1/_2$ calculations. The calculated N_1-N_2 and C_3-N_4 bond lengths increase as compared to that of the corresponding neutral molecules, while the N_2-C_3 bond length decreases (see Table 4). These variations are in agreement with a ligand-centered reduction. It is important to note that in the optimized structures of the square planar monoanions the bond distances within the two metallarings are identical. This indicates delocalization of the added electron over the two ligands. These results can be explained by considering the LUMO of the neutral molecules ($3b_g$-(π^*)) shown in Figure 14. This orbital, corresponding to the antisymmetric combinations of the SOMO of the free π-radical anions, is indeed mainly ligand centered with a small metal contribution. Upon reduction, it becomes singly occupied. The antibonding character of this orbital between N1 and N2 and also C3 and N4 and bonding character between N2 and C3 thus explains the observed bond length modifications. This also explains the increase of the average Ni−N bond distance from 1.840 Å to 1.864 Å because population of this orbital reduces the metal π-back-bonding donation. This MO is metal-to-ligand antibonding in character. Thus, the calculations are in agreement with a ligand-centered reduction in the case of the square planar complexes. The dihedral angle between the two NCNNNi metallacycles

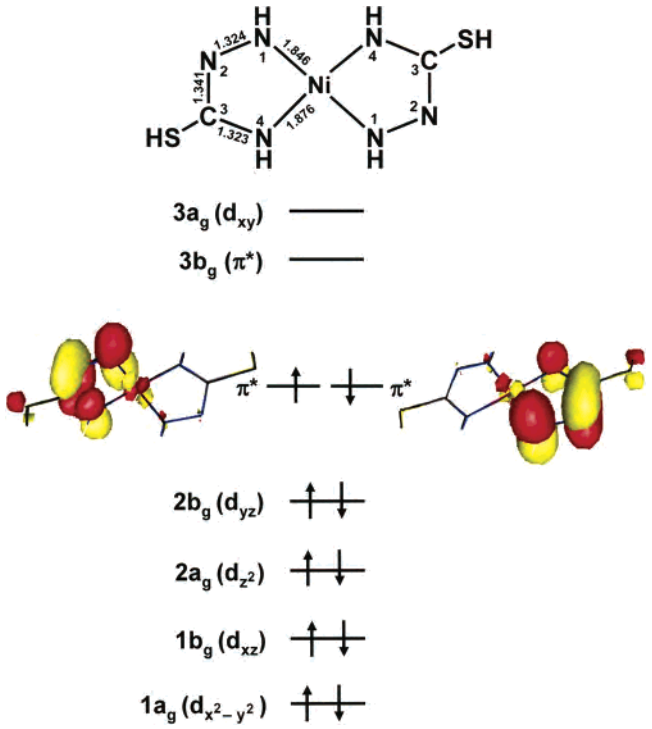

Figure 14. Optimized bond distances (Å) for square planar [Ni($L^{\bullet}_{calcd}$)$_2$] and qualitative MO diagram derived from DFT calculations at the B3LYP/TZV(P) level.

in [Ni($L^{1\bullet}$)$_2$] increases slightly upon reduction, whereas in [Ni^{II}(L_{calc})$_2$]$^-$ these two metallacycles remain to be coplanar.

2. Electronic Structure of the Square Planar Complexes. The electronic structure of the SP nickel complexes is very similar to that of other Ni(II) square planar complexes containing two ligand radicals.[20] In the case of the truncated model, the overall geometry possesses C_{2h} symmetry, which will be used for the nomenclature of the orbitals, the *z* axis being chosen perpendicular to the plane of the molecule, the *x* axis being along the Ni−N1 direction (Figure 14). A qualitative MO diagram, obtained from the BS B3LYP calculation, is shown in Figure 14. Four doubly occupied MOs are mainly centered on the nickel ion, while the empty LUMO+1 orbital is a Ni d_{xy} orbital. Thus, in this complex, the nickel ion is best described as a low-spin d^8 system. The HOMO and the LUMO orbitals correspond to the symmetric and antisymmetric combinations of the SOMO orbitals of the free π-radical anions ($L^{\bullet}_{calc}$)$^-$ ligand, respectively. The LUMO displays ∼8% Ni-3d character.

For the analysis of the spin coupling, it is advantageous to change to an alternative set of MOs, i.e., the corresponding orbitals.[27] This set of orbitals shows most clearly the involved spin couplings since it will transform the orbitals in the spin-up and the spin-down sets such that the most similar possible pairs result. In practice, this means that one finds spin-up and spin-down pairs with an overlap of essentially unity (within 10^{-3}−10^{-4}) and one spin-coupled pair with an overlap between 0 and unity. For the latter, the larger the overlap within the spin-coupled pair, the stronger the electronic coupling between the spin-carrying fragments. The mutual overlap of these two ligand-centered orbitals is 0.40, which correlates with a strong antiferromagnetic interaction between the two organic radicals. This exchange interaction parameter is best estimated through Yamaguchi's formula (eq 4,[28] $\hat{H}_{HDvV} = -2J\hat{S}_A\hat{S}_B$) and is calculated to be ∼ −1660 cm^{-1}.

The electronic structure of the [Ni($L^{1\bullet}$)$_2$] complex is essentially similar to that of the truncated model, with an overlap of the two ligand-centered π-orbitals of 0.63 leading to an antiferromagnetic interaction between the two ligand radicals of about −1800 cm^{-1}.

$$J = -\frac{E_{HS} - E_{BS}}{\langle S^2\rangle_{HS} - \langle S^2\rangle_{BS}} \tag{4}$$

Note that the spin-expectation value is directly related to the corresponding orbital overlap eq 5:

$$\langle S^2\rangle_{BS} = \left(\frac{N^\alpha - N^\beta}{2}\right)\left(\frac{N^\alpha - N^\beta}{2} + 1\right) + N^\beta - \sum_i n_i^\alpha n_i^\beta |S_{ii}^{\alpha\beta}|^2 \tag{5}$$

where $N^{\alpha,\beta}$ are the number of spin-up and spin-down electrons, $n_i^{\alpha,\beta}$ are the individual spin-up and spin-down occupation numbers, and the sum over *i* extends over the corresponding orbital pairs with $S_{ii}^{\alpha,\beta}$ being the spatial overlap integral for the *i*th pair. In the strong interaction limit $S_{ii}^{\alpha,\beta} \rightarrow 1$ the BS solution represents a pure spin state. In the weak interaction limit $S_{ii}^{\alpha,\beta} \rightarrow 0$ and the BS state represents a mixed spin state that requires a multideterminant wave function in a more concise electronic structure description (see below). However, eq 4 involving the spin expectation values neatly takes care of the two interaction extremes and has been shown to be a reasonable approximation over the whole domain of interaction strengths.[28] The strength of the antiferromagnetic interaction is reflected in the value $|S_{ii}^{\alpha,\beta}|^2$.

3. SORCI Calculations of the Truncated Square Planar Model. The relatively small size of the truncated square planar model allows the application of a correlated ab initio method for a more rigorous description of the multiconfigurational ground state of diradical complexes. In the present work, we have used the recently developed SORCI method.[18b] This method can be thought of as a simplified version of the multireference difference dedicated configuration interaction (DDCI3) approach of Malrieu, Caballol, and coworkers,[29] which has shown excellent accuracy in the application to magnetically coupled transition metal dimers.[30] For details of the methodology and a discussion about the necessary active space, we refer to our previous work.[20] In the present SORCI calculations, we have used a slightly

(27) (a) Amos, A. T.; Hall, G. G. *Proc. R. Soc. Ser. A* **1961**, *263*, 483. (b) King, H. F.; Stanton, R. E.; Kim, H.; Wyatt, R. E.; Parr, R. G. *J. Chem. Phys.* **1967**, *47*, 1936. (c) Neese, F. *J. Phys. Chem. Solids* **2004**, *65*, 781.

(28) (a) Yamaguchi, K.; Takahara, Y.; Fueno, T. In *Applied Quantum Chemistry*; Smith, V. H., Eds.; Reidel: Dordrecht, 1986; p 155. (b) Soda, T.; Kitagawa, Y.; Onishi, T.; Takano, Y.; Shigeta, Y.; Nagao, H.; Yoshioka, Y.; Yamaguchi, K. *Chem. Phys. Lett.* **2000**, *319*, 223.

(29) (a) Miralles, J.; Daudey, J. P.; Caballol, R. *Chem. Phys. Lett.* **1992**, *198*, 555. (b) Miralles, J.; Castell, O.; Caballol, R.; Malrieu, J. P. *Chem. Phys. Lett.* **1993**, *172*, 33.

larger than the minimal CAS(2,2) reference space required in the square planar case to be able to describe the three competing singlet, triplet, and quintet spin states. This demanded a CAS(6,5) active space. In agreement with the experimental results, the SORCI method predicts a singlet ground state for the square planar geometry and a coupling constant of $J_{SORCI} = -1353$ cm^{-1} in reasonable agreement with the DFT results (-1600 cm^{-1}). The diradical character estimated through eq 4 of ref 20 was found to be ~33%. The quintet state was predicted considerably higher at 13380 cm^{-1} for the square planar geometry.

4. Calculations on the Monoanions. For the monoanions of square planar complexes **1**−**3**, the EPR spectra are very similar to those of the monoreduced form of other Ni(II) square planar species containing two ligands in a radical form:[19] they display an unusually large g-anisotropy for organic centered radicals. On the basis of our previous DFT calculations,[26] this g-anisotropy can be understood by considering the SOMO of these monoreduced species: upon reduction, one electron populates the LUMO of the neutral complexes. Note that in this case, no broken symmetry calculation is necessary and the BP86 and B3LYP $S = {}^1/_2$ open shell calculations give quite similar electronic structures.

The SOMO orbital possesses b_g symmetry and is mainly ligand-centered (π^*). However, because of that symmetry, it can mix with the out-of-plane d_{xz} and d_{yz} orbitals of the Ni(II) center. Thus, the SOMO possesses significant metal character leading to a ground state with sizable orbital angular momentum due to mixing with low lying d−d excited states of the same symmetry. The latter explains the observed g-anisotropy for the monoanions of **1**−**3**. Indeed, the calculated principal values of the g-tensor, 2.077, 2.014, and 1.99 for the reduced square planar $[Ni(L_{calc})(L_{calc}^{\bullet})]^-$, and 2.058, 2.006, and 2.001 for $[Ni(L^1)(L^{1\bullet})]^-$, are in excellent agreement with the experimental ones (Table 6).

As the SOMO is ligand centered, one could expect to observe hyperfine interactions of the electronic spin with the nitrogen nuclear spins. However, no hyperfine was detected in the experimental spectra. The calculated nitrogen hyperfine couplings for the truncated $[Ni(L_{calc})(L_{calc}^{\bullet})]^-$ model are 30, 2, and 2 MHz for N_1, 20, 1, and 1 MHz for N_4 , and 4 MHz, −2 MHz and −2 MHz for N_3, along the g-tensor axis. It is very likely that these weak hyperfine couplings are hidden in the line width of the transitions.

5. Optimized Geometries of the Neutral Tetrahedral Species. Assuming that the tetrahedral complexes are featuring a high-spin Ni(II) ion and two ligand radicals led us to optimize the ground-state geometry for both high-spin S = 2 and BS $M_s = 0$ states.

Again, in the case of the BP86 functional no BS solutions exist for the calculations on $[Ni(L^{5\bullet})_2]$ and $[Ni(L^{6\bullet})_2]$. All calculations converge to closed shell states. Moreover, the calculations performed on the truncated model complex $[Ni(L_{calc}^{\bullet})_2]$ with the BP86 functional starting from a tetrahedral geometry converged back to the square planar closed shell state obtained before. Thus, these calculations will not be further discussed.

In contrast, all the B3LYP calculations led to BS $M_s = 0$ states lower in energy than the corresponding high-spin S = 2 states. In all cases, the calculated N1−N2, N2−C3 and C3−N4 bond lengths are in excellent agreement with the presence of two ligand radicals coordinated to a Ni^{II} center ion. Moreover, the experimental trends in bond length variations as a function of the geometry are accurately predicted by these calculations, as shown by the lengthening of the average Ni−N and N2−C3 bond lengths together with the shortening of the N1−N2 distances on going from a square planar geometry to the tetrahedral one.

The calculated dihedral angle between the two NNCCNNi metallocycles is slightly twisted at 82° in the tetrahedral $[Ni(L_{calc}^{\bullet})_2]$ case, where in an ideal tetrahedron this angle would be 90°. In the case of $[Ni(L^{5\bullet})_2]$, this dihedral angle is accurately reproduced with a calculated value of 86° as compared to an experimental one of 85°, while for $[Ni(L^{6\bullet})_2]$, a larger deviation is observed with a calculated value of 85° compared to the experimental value of 71°.

It is worth noticing that in the case of $[Ni(L^{5\bullet})_2]$ where we performed a B3LYP geometry optimization starting from a square planar environment around the nickel ion, the calculations converged back to a tetrahedral geometry at the Ni(II) center. Thus, in agreement with the NMR studies where only one isomer was detected in solution, there is no minimum for a (distorted) square planar isomer.

6. Electronic Structure of Tetrahedral $[Ni(L_{calc}^{\bullet})_2]$, $[Ni(L^{5\bullet})_2]$, $[Ni(L^{6\bullet})_2]$ Complexes. In the tetrahedral cases, the B3LYP calculations show that the lowest energy spin-unrestricted solution is of $M_s = 0$ BS type. The results are similar for all three calculations performed. We will therefore focus on the analysis of the electronic structure of tetrahedral $[Ni(L_{calc}^{\bullet})_2]$.

A qualitative bonding scheme derived from the B3LYP BS $M_s = 0$ calculation of tetrahedral $[Ni(L_{calc}^{\bullet})_2]$ is shown in Figure 15. Five occupied orbitals of mainly nickel in character are identified. Three of these orbitals (not shown), two from the e set and one from the t_2 set, are found in the spin-up as well as the spin-down manifold and are therefore doubly occupied. The other two nickel-based orbitals originate from the t_2 set and occur only in the spin-up manifold. These orbitals are thus singly occupied with parallel spins. This orbital occupation pattern defines a high-spin Ni(II) configuration ($S_{Ni} = 1$) at the metal center. In addition to these two metal-centered orbitals, two ligand-centered orbitals are identified in the spin-down manifold that are not populated in the spin-up manifold, thus leading to the observed overall $M_S = 0$ BS state. These two orbitals correspond mainly to two symmetry-adapted combinations of the SOMO of the two ligand radicals. Thus, the basic electronic structure description features a high-spin Ni(II) ion that is strongly antiferromagnetically coupled to two

(30) (a) Calzado, C. J.; Sanz, J. F.; Malrieu, J. P.; Ilas, F. *Chem. Phys. Lett.* **1999**, *307*, 102. (b) Calzado, C. J.; Malrieu, J. P. *Chem. Phys. Lett.* **2000**, *317*, 404. (c) Calzado, C. J.; Sanz, J. F.; Malrieu, J. P. *J. Chem. Phys.* **2000**, *112*, 5158. (d) Calzado, C. J.; Cabrero, J.; Malrieu, J. P.; Caballol, R. *J. Chem. Phys.* **2002**, *116*, 2728. (e) Calzado, C. J.; Cabrero, J.; Malrieu, J. P.; Caballol, R. *J. Chem. Phys.* **2002**, *116*, 3985. (f) Castell, O.; Caballol, R. *Inorg. Chem.* **1999**, *38*, 668.

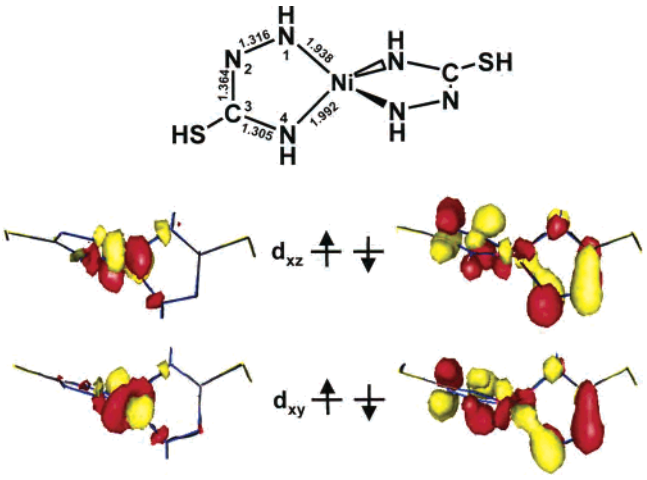

Figure 15. Optimized bond distances (Å) of tetrahedral $[Ni^{II}(L^{\bullet}_{calcd})_2]$ and qualitative MO diagram of the corresponding orbitals of magnetic pairs calculated at the B3LYP/TZV(P) level.

ligand-centered π-radicals as has originally been proposed by the authors of ref 7.

This is also confirmed by the corresponding orbital analysis, where one finds two pairs of orbitals with an overlap between 0 and 1. Both spin-coupled ("magnetic") pairs are formed between a metal centered t_2 orbital and a ligand-centered orbital of the corresponding symmetry, as depicted in Figure 15. The mutual overlaps of these two orbitals for each pair are 0.50 and 0.57, respectively, which indicates in both cases a strong antiferromagnetic interaction. The exchange interaction parameter is calculated to be -1450 cm^{-1}.

In the present case, the result of the corresponding orbital analysis is that there is a strong antiferromagnetic exchange interaction between the $(L_{calc}^{\bullet})^-$ radical ligands and the central nickel via a π-overlap pathway. The calculated strong exchange interaction is consistent with the observed ground-state spin of $S_t = 0$ with no indication of thermal population of the higher lying $S = 1$ or 2 states up to room temperature. However, since the precise values of J are not known from experiment, the accuracy of the calculation cannot be checked.

The calculated energy difference between the square planar (lowest) and tetrahedral form of $[Ni^{II}(L^{\bullet}_{calcd})_2]$ is only $\sim$4 kcal/mol: obviously, the change in geometry from square planar to tetrahedral in this diradical containing Ni(II) complexes is electronically not strongly disfavored. Note that in this instance steric interactions between the two ligands are not involved. This is different for $[Ni(L^{5\bullet})_2]$ and $[Ni(L^{6\bullet})_2]$ where square planar forms do not exist in silico. The electronic structures of these two species are very similar to that of tetrahedral $[Ni(L^{\bullet}_{calcd})_2]$ described above. The overlaps of 0.49 and 0.47 for **5** and 0.52 and 0.50 for **6** of the two corresponding orbital pairs lead to calculated coupling constants, J, of -950 and -1080 cm^{-1}, respectively.

7. SORCI Calculations on the Truncated Tetrahedral Model. The SORCI calculations on the tetrahedral species $[Ni^{II}(L^{\bullet}_{calc})]$ were carried out analogously to the calculations on the square planar structure. For the tetrahedral species a CAS(4,4) reference space was used, which is the minimum needed to describe the first singlet, triplet, and quintet states. The four orbitals are two metal-based t_2 derived MOs and two ligand orbitals and were generated by a spin-restricted B3LYP calculation on the quintet state. The calculations are again in agreement with experiment in predicting a singlet ground state with the next triplet state lying at 2751 cm^{-1}. From this, a J_{SORCI} of -1357 cm^{-1} is obtained which is, again, in excellent agreement with the B3LYP prediction. The first quintet state is calculated at 10541 cm^{-1}, which is slightly larger than predicted by the spin-coupling model for two $S = 1$ units ($6J_{SORCI} = 8142$ cm^{-1}).[31]

8. Optimized Geometries of the Monoreduced Tetrahedral Species. B3LYP DFT calculations of the monoreduced forms of these tetrahedral species were also performed. Upon reduction in silico of the tetrahedral $[Ni(L^{\bullet}_{calc})_2]$ model, no minimum for a monoanion with tetrahedral geometry can be found. The structure converges back to square planar. However, a B3LYP BS $M_s = {}^1/_2$ optimized tetrahedral geometry was found for the monoreduced species of $[Ni(L^{6\bullet})_2]$.

In this case, the tetrahedral geometry is conserved, as indicated by the dihedral angle between the two NNCNNi metallacycles of 78° for $[Ni(L^6)(L^{6\bullet})]^-$. Lengthening of the average N1−N2 and C3−N4 bond distances with the corresponding shortening of the N2−C3 is indicative of a ligand-centered reduction. In contrast to the square planar monoreduced species where the additional charge is fully delocalized over the two ligands, the one-electron reduction process appears here to be much more localized on one ligand: the corresponding C−N and N−N bond distances of the two ligands in $[Ni(L^6)(L^{6\bullet})]^-$ are no longer identical (see Figure 16). One ligand features a long N1−N2 bond at 1.381 Å, a short N2−C3 bond at 1.302 Å, and a long C3−N4 at 1.355 Å, which are characteristic of a fully reduced $(L^6)^{2-}$ ligand, whereas the other ligand displays bond lengths characteristic of the $(L^{6\bullet})^-$ radical form of the ligand.

9. Electronic Structure of the Monoreduced Tetrahedral Species $[Ni(L^6)(L^{6\bullet})]^-$. The lowest energy, spin-unrestricted solution for the monoreduced tetrahedral species is a BS $M_s = {}^1/_2$ solution. As described for the neutral case, we identify five occupied orbitals that are mainly metal in character. Three of these are found in both the spin-up and

(31) The singlet wave function is quite complicated having 62% contribution of the closed shell configuration and 11% from double excitations in the active space, 2% contribution from the configuration with four open shells and still 2% contribution from the quadruple excitation within the active space. Thus, the first-order interacting space of this calculation included up to hextuple excitations relative to the closed shell configuration, which shows that a multireference treatment is hardly avoidable in predicting the ground-state properties of such complicated spin-coupled molecules from correlated ab initio methods. The only state with a simple configurational structure is the quintet state. The population analysis of the correlated density shows indeed 1.8 unpaired electrons on the nickel center and two unpaired electrons delocalized over the ligands, which is in support of the DFT results.

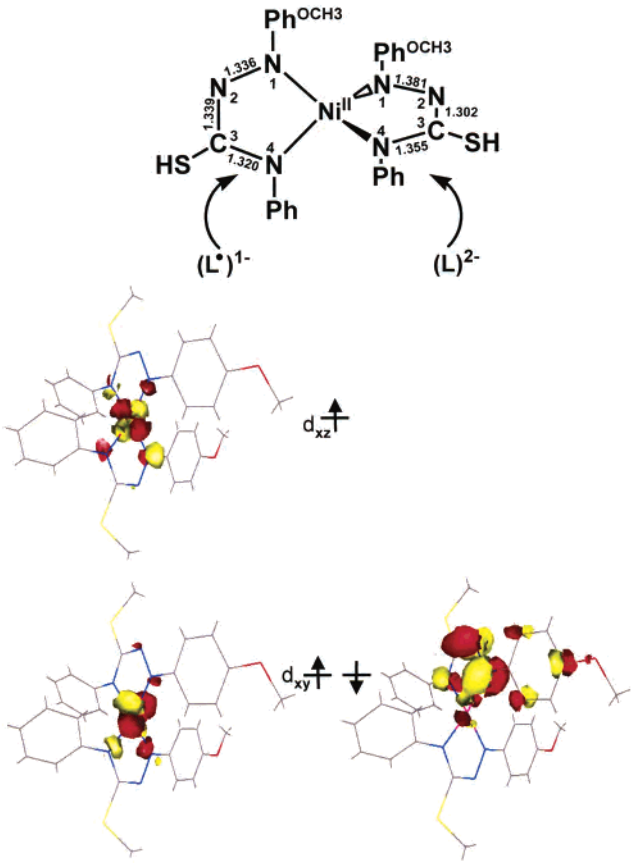

Figure 16. Optimized geometry of tetrahedral $[Ni^{II}(L^6)(L^{6\bullet})]^-$ and qualitative MO diagram of the magnetic orbitals derived from B3LYP/TZV(P) calculations.

spin-down manifolds and are thus doubly occupied, while two are only populated in the spin-up manifold. Thus, upon reduction of the complexes the oxidation state of the metal center did not change: it is still best described as a high-spin nickel(II) ion ($S = 1$). In addition, one finds one ligand-centered orbital which is only occupied in the spin-down manifold. This overall occupation pattern leads to the $M_s = {}^1/_2$ BS state. Thus, the basic electronic description of the reduced species features a high-spin Ni(II) strongly antiferromagnetically coupled to a single localized ligand-centered π-radical.

This description is confirmed by the corresponding orbital analysis of $[Ni(L^6)(L^{6\bullet})]^-$ shown in Figure 16. It is obvious from this figure that the unpaired electron is localized at the metal center. Moreover, in the magnetic pair, the spin density on the organic part is localized on one ligand only. In conjunction with the bond length differences between the two ligands in the optimized geometries, this clearly indicates that this monoanionic complex possesses two ligands in different oxidation states, namely, the fully reduced dianionic $(L^6)^{2-}$ closed shell form and the π-radical monoanionic $(L^{6\bullet})^-$ form, with little electronic delocalization of the extra electron from the fully reduced form to the monoreduced one.

Thus, all calculations are in agreement with ligand-centered reduction processes leading to $S_t = {}^1/_2$ complexes, the doublet state resulting from the antiferromagnetically coupling of a high-spin Ni(II) with one ligand radical.

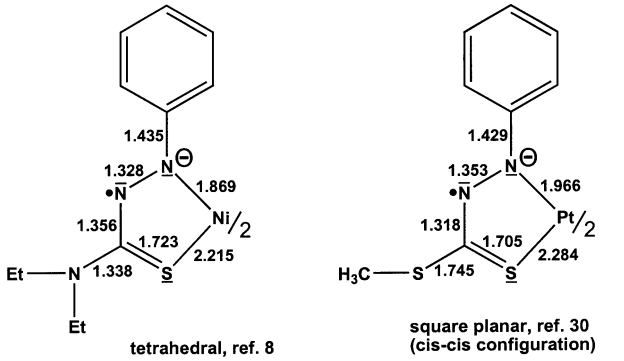

Figure 17. Structure and bond distances (Å) of a tetrahedral nickel(II) and a square planar platinum(II) complex from refs 8 and 33, respectively.

As it has been discussed previously,[32] it is possible to calculate reasonable g-tensors for antiferromagnetically coupled dimers from DFT calculations. The main idea of this approach is to determine the g-tensors corresponding to the high-spin and broken symmetry states and then to extract from these calculations hypothetical site-*g*-tensors. Coupling the latter by using the usual vector coupling model then yields a g-tensor reflecting the properties of the antiferrromagnetic state. Applying this methodology, we calculated the g-tensor for $[Ni(L^6)(L^{6\bullet})]^-$, which has principal values of $g_x = 2.037$, $g_y = 2.198$, and $g_z = 2.205$, which leads to $g_{iso} = 2.147$. This tensor displays a large anisotropy, in agreement with a metal-centered $S = {}^1/_2$ species. The g_{iso} value is surprisingly close to that of the **a** subspecies identified in the spectra of electrochemically generated $[Ni(L^6)(L^{6\bullet})]^-$ but compares also well with that of the **b** subspecies (Table 6). Compared to the experimental data for these two subspecies, the calculated *g*-tensor is more axial. However, the dihedral angle between the two $\overline{NNCNN}$i metallacycles is an important parameter for the g-anisotropy which has not yet been determined experimentally. The present results may be compatible with our proposal that the two subspecies **a** and **b** observed experimentally correspond to an equilibrium between two different distorted tetrahedral isomers.

Discussion

For complexes **1**−**3** spectroscopic evidence such as an intense LLCT band, the X-ray structure determination of **1**, and the theoretical calculations clearly establish that the complexes are diamagnetic square planar nickel(II) complexes with two ligands in their π-radical monoanionic form. The diamagnetic ground state of these complexes originates from a strong antiferromagnetic interaction between the two radical ligands. These species are singlet diradicals as has been determined for bis(*o*-phenylenediamine radical)nickel(II) complexes.[19,20] From correlated ab initio calculations, we conclude that they have ~33% diradical character.

(32) (a) Slep, L. D.; Mijovilovich, A.; Meyer-Klaucke, W.; Weyhermüller, T.; Bill, E.; Bothe, E.; Neese, F.; Wieghardt, K. *J. Am. Chem. Soc.* **2003**, *125*, 15554. (b) Sinnecker, S.; Neese, F.; Noodleman, L.; Lubitz, W. *J. Am. Chem. Soc.* **2004**, *126*, 2613.

Table 7. Optimized Bond Distances (Å) of Square Planar and Tetrahedral Neutral and Monoanionic Complexes

complex	method	av. N_1-N_2[a]	av. N_2-C_3	av. C_3-N_4	av. Ni−N	θ, deg
			square planar geometry			
$[Ni(L^{\bullet}_{calcd})_2]$	B3LYP, BS	1.324	1.341	1.324	1.861	0
$[Ni^{II}(L^{1\bullet})_2]$	BP86	1.348	1.346	1.336	1.862	22
	B3LYP	1.337	1.337	1.319	1.891	19
	exp	1.343	1.339	1.321	1.847	12
$[Ni(L_{calcd})_2]^{1-}$	B3LYP	1.362	1.310	1.349	1.864	0
$[Ni(L^1)_2]^{1-}$	BP86	1.385	1.318	1.344	1.880	29.4
	B3LYP	1.379	1.306	1.1.380	1.889	22.5
			tetrahedral geometry			
$[Ni(L^{\bullet}_{calcd})_2]$	B3LYP, BS	1.316	1.364	1.305	1.966	82
$[Ni^{II}(L^{5\bullet})_2]$	BP86	1.342	1.341	1.345	1.891	53.5
	exp	1.333	1.352	1.325	1.904	85
$[Ni^{II}(L^{6\bullet})_2]$	B3LYP, BS	1.327	1.346	1.321	1.977	85
	BP86	1.342	1.344	1.340	1.903	65
	exp	1.343	1.346	1.328	1.891	71
			tetrahedral geometry			
$[Ni(L^5)_2]^{1-}$	BP86	1.370	1.323	1.354	1.908	55
	B3LYP, BS[b]					
$[Ni(L^6)_2]^{1-}$	BP86	1.365	1.327	1.352	1.939	
	B3LYP, BS[b]	1.336	1.339	1.320	2.025	
		1.381	1.302	1.355	1.952	

[a] Labeling see Figure 13. [b] Two inequivalent ligands $(L^{6\bullet})^{1-}$ and $(L^6)^{2-}$.

In contrast, complexes **5** and **6** adopt a tetrahedral geometry. Again, the bond lengths within the ligands clearly indicate the presence of two π-radical monoanions in each complex. A similar tetrahedral structure has been deduced for **4** from spectroscopy. DFT calculations performed on these tetrahedral complexes clearly establish that the metal ion is nickel(II) in a high-spin configuration ($S = 1$) and that the diamagnetism of these three molecules results from a strong antiferromagnetic coupling with two ligand radicals.

Electronic spectroscopic studies on the reduced monoanionic species $[\mathbf{1}]^-$, $[\mathbf{2}]^-$, and $[\mathbf{3}]^-$ indicate that in these complexes the square planar $Ni^{II}N_4$ unit is retained. An intense LLCT band at 1100−1400 nm is indicative of complete delocalization of the excess electron over both ligands.

In the dianionic species $[\mathbf{1}]^{2-}$, $[\mathbf{2}]^{2-}$, and $[\mathbf{3}]^{2-}$ the above SOMO becomes a ligand-centered HOMO. Thus, the square planar neutral, monoanionic, and dianionic forms of complexes **1**, **2**, and **3** contain each a diamagnetic nickel(II) ion ($d,^8$ $S = 0$) in a square planar ligand field and (a) two monoanionic π-radicals and (b) a class III mixed valent ligand system $[(L^{1-3\bullet})^{1-}M(L^{1-3})^{2-}]^{1-} \leftrightarrow [(L^{1-3})^{2-}M(L^{1-3\bullet})^{1-}]^{1-}$, and (c) two closed-shell dianionic ligands, respectively.

In stark contrast, complexes **4**, **5**, and **6** containing 1,4-diphenyl derivatives of the *S*-methyl-isothiosemicarbazides are distorted tetrahedral. The electronic structures of these neutral complexes must be described as species with a central high-spin nickel(II) ion ($d,^8$ $S = 1$) and two N,N-coordinated π-radical monoanions. The radical spins couple strongly intramolecularly in an antiferromagnetic fashion with the two t_2 metal d orbitals each containing an unpaired electron ($S = 0$). DFT calculations have shown that the energetic difference between a tetrahedral and a square planar arrangement of the ligands is small ($\sim$4 kcal mol^{-1}) if no steric hindrance comes into play.

Interestingly, the paramagnetic monoanions $[\mathbf{4}]^-$, $[\mathbf{5}]^-$, and $[\mathbf{6}]^-$ ($S = {}^1/_2$) display EPR spectra with a significantly larger g-anisotropy than that observed for the square planar analogues $[\mathbf{1}]^-$, $[\mathbf{2}]^-$, and $[\mathbf{3}]^-$. In addition, there are always two subspectra observed for $[\mathbf{4}]^-$, $[\mathbf{5}]^-$, and $[\mathbf{6}]^-$, which led us to propose two tetrahedral geometric isomers A and B (Scheme 5) for each of these species. The electronic spectra of the tetrahedral monoanions lack the intense MVCT band $>$ 1100 nm observed for the square planar monoanions. This observation and the results of the DFT calculations allow us to conclude that the excess electron is localized on one ligand monoanion. Thus, their electronic structure is best described as tetrahedral $[Ni^{II}(L^{4-6\bullet})(L^{4-6})]^-$ where a high-spin Ni(II) ion ($d,^8$ $S = 1$) couples antiferromagnetically with a ligand π-radical. The structure of the dianions $[Ni(L^{4-6})_2]^{2-}$ remains unclear due to the lack of a crystal structure determination.

Revenco and Gerbeleu et al. had shown[1-5] that oxidation of **1** with iodine affords **7** an octahedral complex of Ni^{II} with two neutral ligands ($L^{1,ox}$) and two in trans-position relative to each other coordination iodide ligands. We have discovered that the analogous oxidation of tetrahedral **5** yields complex **9**, which again contains two oxidized ligands ($L^{5,ox}$) and two in trans-position coordinated $(I_3)^-$ ligands. Apparently, the two organic ligands in the NiN_4 plane do not experience steric hindrance (repulsion). To the contrary, intramolecular π-stacking between the ligands is observed. This experimental result seems at first glance to contradict the notion that the tetrahedral NiN_4 polyhedron in complexes **4**−**6** is the result of steric hindrance between two 1,4-diphenyl-isothiosemicarbazide derivatives in a planar NiN_4 coordination mode. DFT calculations have shown that in sterically unhindered 1-phenyl systems (**1**−**3**) the planar geometry is more stable by 4 ± 3 kcal mol^{-1} than the tetrahedral. Thus, the energetic difference based on electronic effects alone between the two geometries is small. It is interesting to note in this context that the structure of bis-(*N*,*N*-diethylphenylazothioformamide)nickel(II)[8] is tetrahedral, whereas the very similar platinum(II) complex bis-

(methyl-*N*′-phenyldiazenecarbodithioato)platinum(II) shown in Figure 17 is planar.[33] Both complexes have the same five-membered chelate rings $\overline{\text{M}-\text{S}-\text{C}-\text{N}-\text{N}}$. Here, of course the larger crystal field stabilization energy of a diamagnetic Pt(II) ion (d^8, $S = 0$) favors the square planar arrangement over a tetrahedral one. As pointed out previously, the π-stacking interaction between the phenyl rings in a putative square planar $[Ni^{II}(L^{5\bullet})_2]$ may become as short as ~2.8 Å where this interaction may be repulsive rather than attractive.

Acknowledgment. This work was financially supported by the Fonds der Chemischen Industrie.

Supporting Information Available: Figures S1−S7 and X-ray crystallographic files for compounds **1** and **5**−**11**. This material is available free of charge via the Internet at http://pubs.acs.org.

IC040117E

(33) Dessy, G.; Fares, V. *Acta Crystallogr.* **1980**, *B36*, 2266.